# Microstructure and poro-mechanical performance of Haubourdin chalk

Nadah Jaouad, F. Bignonnet, Catherine A. Davy, Frédéric Skoczylas, David Troadec, S. Bakowski

# Microstructure and poro-mechanical performance of Haubourdin chalk

Jaouad Nadah[a,b] , F. Bignonnet[a,c,d] , C.A. Davy[a,b,*], F. Skoczylas[a,b] , D. Troadec[e] , S. Bakowski [f]

a Laboratoire de Mécanique de Lille (LML) UMR8107, France
b Ecole Centrale de Lille, BP 48, F-59651 Villeneuve d'Ascq Cedex, France
c Ecole Nationale des Ponts et Chaussées (ENPC), France
d LMSGC/Institut Navier, Cité Descartes 6-8, avenue Blaise Pascal, 77455 Marne-la-Vallée Cedex 2, France
e Institut d'Electronique, de Microélectronique et de Nanotechnologie (IEMN), UMR8520, Avenue Poincaré, BP 60069, 59652 Villeneuve d'Ascq, France
f Eurovia Management, Délégation Technique Nord, Port Fluvial 4ème Avenue, 59120 Loos, France
* Corresponding author at: Ecole Centrale de Lille, BP 48, F-59651 Villeneuve d'Ascq Cedex, France.
Tel.: +33 320335363; fax: +33 320335353. E-mail address: catherine.davy@ec-lille.fr (C.A. Davy).

## Abstract

Large chalk deposits are to be found in the North of France, and, as a result, developing chalk as a load-bearing aggregate is considered by French road building companies. Due to its limited mechanical performance, chalk is subjected to a medium heat treatment process (up to 500 °C). In this context, microstructure and poro-mechanical performance of Haubourdin chalk are characterized before and after heat treatment. The investigation of the so-called water weakening effect is associated to that of heat-treatment, mainly to show to what extent the strength of Haubourdin chalk decreases at a given water saturation state, prior to or after heat-treatment.

In terms of microstructure analysis, SEM and FIB/SEM observations show the initial weak cementation of Haubourdin chalk, in direct relation with its moderate mechanical performance. After heat treatment, minor re-crystallisation of calcium carbonate is observed, which should be confirmed further.

The specific behavior of Haubourdin chalk is highlighted under partial water saturation and after heat treatment, by using uniaxial compressive tests, and triaxial drained and undrained compressive tests. Pore collapse is quantified directly under increasing hydrostatic stress by measuring coupled gas permeability and porosity change. A heat-hardening effect is identified, which is counter-balanced by the water-weakening effect. The latter makes natural Haubourdin chalk unsuitable as load-bearing road aggregate, without further binding matter.

### Highlights

► Haubourdin chalk has undergone very limited diagenesis processes. This is confirmed by its high Biot coefficient of 0.88, consistent with the literature.

► At 100% saturation, Haubourdin chalk loses up to 45% of its reference dry strength (water weakening effect).

► After 500 °C heat-treatment, uniaxial compressive strength increases significantly, by 47.6% (heat hardening effect). This is lost after a small 1.5% re-saturation.

► Pore collapse under hydrostatic stress is identified at 20 MPa (dry reference state): it is affected by water weakening, and improved by heat hardening.

# Keywords

Chalk ; Microstructure ; Mechanical performance ; Poro-mechanics ; Water saturation ; Heat treatment


# 1. Introduction

Pelagic carbonate deposits are abundant in Western Europe, and particularly in the North of France. They have been widely investigated in petroleum science [1], [2], [3], [4], [5], as they constitute the source rock of industrially exploited off-shore oil reservoirs, mainly in the North Sea area [6]. Over various geological periods of time, plankton algae and protozoan foraminifera accumulate and form sedimented calcareous ooze. By burial diagenesis, ooze develops into weakly consolidated rock, namely chalk, and then into limestone [5]. Being deposited in successive layers, ooze, and then, chalk may show anisotropy, related to the existence of bedding planes [7]. Diagenetic mechanisms, which contribute to chalk formation, are a combination of mechanical compaction, micro-fossil recrystallisation, and also, in minor proportion, calcitic grain cementation [8], [2], [6]. One major mechanism involved in $CaCO_3$ cementation is the dissolution/recrystallisation of calcium carbonate from its ions ($Ca^{2+}$ and $CO_3^{2-}$), which are generally present in the interstitial pore water [9], [10]. Extensive cementation of calcitic grains leads to the formation of stronger rock, i.e. limestone. While reservoir chalk may be buried down to a depth of 3000 m, chalk also outcrops at the ground surface, which eases its microstructural and mechanical characterization, see [6].

In the North of France, chalk has been used for decades in Civil Engineering for earthworks and roads. In such instances, chalk is generally added with hydraulic binders in order to achieve sufficient mechanical performance. Indeed, although several million cubic meters of chalk are used each year [11], its peculiar mechanical behaviour does not allow for extensive valorization. As for silts, the main drawback in using chalk as a civil engineering material is its ability to liquefy under the combined presence of mechanical stress and water [8], [3], [12].

In this contribution, our main objective is to investigate whether the mechanical performance of Haubourdin chalk can be improved (or not) by a mild heat-treatment of up to 500 °C, independently of subsequent partial water re-saturation. As chalk decarbonation is reputed to occur from 600 °C upwards [13], no higher heat-treatment temperature has been investigated. It is inferred that such heat treatment could permanently change the chalk properties, and in particular bring some cementation between calcite grains. Indeed, a controversy still exists as to whether chalk mechanical performance is mainly driven by capillary pressure, even above 100 °C, or if it is rather controlled by dissolution/recrystallisation of calcium carbonate [8], [9], [3], [10]. Besides, it is thought that the heat treatment could affect calcite itself, or the clays and possibly the silica phases in the material. Although these are minor constituents, an effect may be expected as they contribute a significant part of the specific surface. Furthermore, this study is considered as an opportunity to investigate chalk microstructure by varying experimental means, and to provide arguments as to the microstructural changes, which chalk sustains after heat treatment.

More precisely, we characterize experimentally the microstructure and mechanical performance of Haubourdin chalk under uniaxial and triaxial compression (in drained or undrained conditions) in four different successive states: (1) in an initial dry state, taken as the reference dry state; (2) at a uniform partial water-saturation level $S_w$; (3) after a mild heat-treatment of up to 105, 200, 300 or 500 °C and finally (4) after partial water re-saturation of heat-treated chalk.

Although creep is a major phenomenon occurring in geological chalk deposits [5], it is not investigated here: all our experiments are conducted at a sufficient displacement rate, and with sufficiently low stresses, to avoid significant creep. As a matter of comparison, in [5], for chalk of similar porosity to Haubourdin chalk (with a value of 43%), the threshold from which creep strain is considered significant is of 0.1%; this is obtained after 1000 s (ca. 16 min) at 80 MPa. Our uniaxial compressive tests last 1500 s and achieve a strain of 0.1% with stresses below 20 MPa. Moreover, creep has not been considered relevant to this study, where improving the mechanical performance of chalk as road layer aggregate is investigated.

# 2. Material preparation and experimental procedures

## 2.1. Material

### 2.1.1. Chalk origin and sample preparation

The Normat chalk quarry is located near Haubourdin, in the villages of Emmerin and Loos (in the Nord department of France). Two hundred thousand tons are extracted each year, and processed with hydraulic binders to produce aggregates for road capping layers. The open-air deposit is composed of Upper Cretaceous (Seno-Turonian) chalk, which is about 90 million years old. Despite being close to the ground surface, Haubourdin chalk does not belong to the thin Quaternary cover, as described by Ziegler geological map of the North Sea area [6], [14]. Such outcropping is possibly due to tectonic movements such as the Alpine orogeny, which has affected chalk to be found as far away as southern England (e.g. in the Whitecliff Bay area, Isle of Wight) [15]. Microstructural investigation of Haubourdin chalk will provide further arguments to assess this, by identifying qualitatively the amplitude of its compaction and recrystallisation, see Section 3.1.1.

Haubourdin chalk is covered by a vegetal soil layer about three meters thick. According to French standards for ballast and capping layer aggregates, its geotechnical classification is as a R12m/R12s rock, which corresponds to medium density material [16]. An early engineering study [17] has identified its average apparent dry density at 1.57 g/cm$^3$±0.05, and its mean water content at 23.0% ±1.3.

For this study, several blocks have been taken manually from the same area after excavator digging, see Fig. 1(a), in order to limit variations in mineralogical composition and mechanical performance. As in most chalk deposits [7], extensive macro-cracking and a few chert inclusions are observed, see Fig. 1(b). Haubourdin chalk may also display orange-colored surfaces parallel to the bedding, see Fig. 1(c). These are attributed to iron oxide/hydroxide originating from ground water seepage, rather than to stylolites as also described in the geology literature [18]. Together with macro-cracks and cherts, these are present sporadically, so that they have been removed from the samples used in this study.

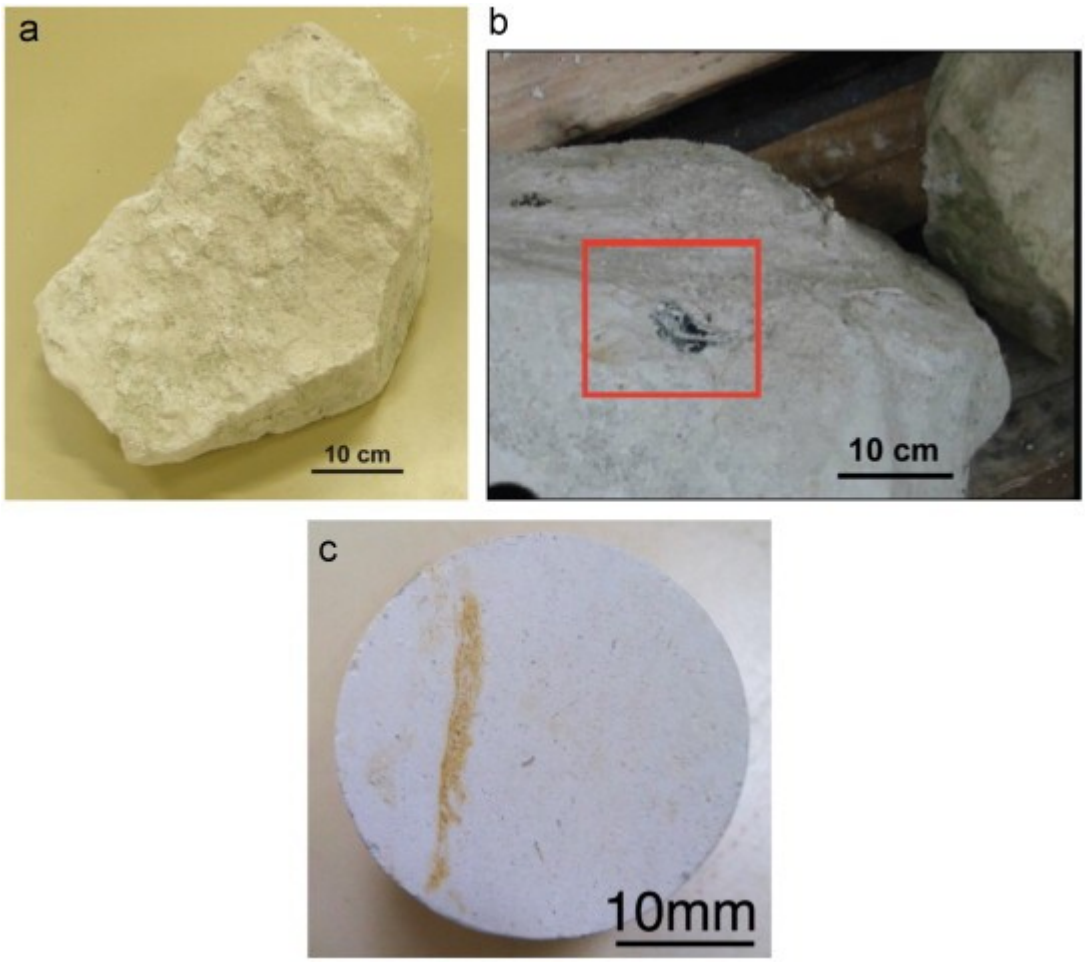


Fig. 1. Typical samples of Haubourdin chalk. Top pictures: two blocks after extraction from the quarry: (a) a very clear, homogeneous and almost white color is observed, together with sharp edges; (b) siliceous inclusions (chert) are present in small amounts. Macro-cracks may also be present within the blocks (not photographed). Bottom picture: (c) top view of a cored chalk sample, displaying a reddish line attributed to iron oxide hydroxide.

Cylindrical samples are made by coring under water, saw cutting and surface grinding in order to obtain parallel end surfaces. Sample final dimensions are of 37.0 mm±0.5 diameter and 75.0 mm±0.5 height, so that they have a height/diameter ratio of ca. 2. During mechanical compressive tests, this aims to avoid frictional end effects (which may occur for height/diameter ratios lower than 2) and buckling (which may occur for height/diameter ratios greater than 2). After being set to adequate dimensions, samples are oven-dried at 60 °C until mass stabilization. As recommended by the European standard for stone materials NF EN 1936, mass stabilization is assumed to have been obtained as soon as two successive measurements, taken at 24 h interval, differ by less than 0.1%.

In total, a number of 54 specimens are used in this study: 16 in the 60 °C oven-dried state, 11 in the partially water-saturated state, five after 10 cycles of water imbibition/60 °C oven-drying, 17 after heat-treatment (in uniaxial or triaxial compression), and five after heat-treatment and partial water saturation. Six reference dry samples are especially preserved in order to assess chalk anisotropy: three are cored along a horizontal plane w.r.t. Haubourdin deposit, and three others have their main axis along the vertical direction. All other samples are cored along an undetermined direction.

### 2.1.2. Water saturation procedures

In order to obtain a fixed and homogeneous (or uniform) water saturation level $S_w$, 10 chalk samples are placed in hermetic chambers each above a different salt-saturated water solution, which enables to obtain a fixed relative humidity (*RH*) in the chamber atmosphere. Depending on the nature of salt, and on temperature, different *RH* are obtained, see [19], and the greater the *RH*, the greater the $S_w$. All tests are performed at ambient temperature, at an average of 20 °C. With Haubourdin chalk, obtained $S_w$ range between 1.0% and 22.0%±0.1.

The effect of full water saturation is also assessed. To do this, nine samples are immersed in water for 8, 30 or 65 days (three samples per duration), and then tested in uniaxial compression until failure.

Finally, after a mild heat treatment up to 60, 105, 200, 300 or 500 °C, five chalk samples (one per temperature) are partially re-saturated in an hermetic chamber using a salt saturated solution (providing 43% *RH*), until reaching a 1.5% saturation level. As explained in the introduction, this aims at investigating whether partial re-saturation weakens Haubourdin chalk, despite mild heat treatment.

### 2.1.3. Heat treatment procedure

The reference dry state for this study is taken at mass stabilization under 60 °C oven-drying. From this starting “reference dry” point, 16 chalk samples are heat-treated by subjecting them to the following heating/cooling kinetics: (1) heating at a rate of 20 °C/h until reaching the target temperature $T_{max}$=105, 200, 300 or 500 °C, depending on the sample; (2) stabilization at $T_{max}$ for 24 h (for 11 samples) or 48 h (for five samples); (3) cooling at a rate of 20 °C/h until reaching room temperature (30 °C). Each sample is subjected to a single $T_{max}$. The heating/cooling rate is chosen at a low value to limit thermal gradients throughout the sample. Then, for all samples kept 24 h at target temperature $T_{max}$, each is covered with a water-tight coating, equipped with strain gauges and tested under uniaxial or triaxial compression, see Section 2.2. Samples kept for 48 h at $T_{max}$ are tested under uniaxial compression without water-tight protection.

## 2.2. Experimental methods

This study comprises two complementary investigations: (1) of chalk microstructure, and (2) of chalk mechanical performance under uniaxial and triaxial compression, before and after partial water-saturation or heat-treatment. A single state is assessed before heat-treatment (or partial water saturation): it is the so-called “reference dry” state, obtained at mass stabilization under 60 °C oven-drying. It should be noted that, after heat-treatment, chalk microstructure is only assessed by 2D image analysis from SEM (Scanning Electron Microscopy) observations, whereas a more comprehensive study is performed in the initial state.

### 2.2.1. Microstructure assessment

The initial microstructure of Haubourdin chalk is identified by a range of methods, as follows.

Mercury Intrusion Porosimetry (MIP) provides apparent and solid densities, pore surface area, median and average pore sizes, pore size distribution and total connected porosity $\phi$. It is performed on two centimetric samples, using a MICROMERITICS AutoPore IV 9500 up to 200 MPa, which corresponds to intruded pores down to 6 nm.

By saturating 10 chalk samples with ethanol under vacuum for 24 h, total connected porosity $\phi$, apparent dry density and solid dry density are measured without dissolving $CaCO_3$, which the use of water would have enhanced. Two sample sizes are used: 19.50 mm±0.12 diameter and 40 mm±2 height, or 35.0 mm ±1.2 diameter and 16.5 mm±2.5 height to check whether this has an effect on $\phi$. Complementarily, helium pycnometry provides chalk solid dry density: we use three block samples of mass ranging from 0.68 and 9.93 g, tested each twice, for up to 6 h helium intrusion.

Bernard calcimetry mixes chalk samples of ca. 0.5 g with dilute HCl, in order to assess their carbonate content by mass comparison with a standard 100% pure $CaCO_3$ sample. Three samples are tested by this method.

The X-ray diffractometry (XRD) analysis provides the mineralogical analysis for both chalk and its non-carbonate residue, obtained after the previous calcimetry test, i.e. generally silica and clay components. A Philips[a] PW 1729 instrument with a copper anticathod ($\lambda$=1.54Å) is used. One sample of chalk and one of its residue are tested by this method.

Thermogravimetry analysis (TGA) enables to determine the actual temperature range, during which water loss and other decomposition phenomena (mainly decarbonation) occur, with a weighing accuracy of ±0.01 mg. Six different powdered chalk samples, with an average mass of 50 mg±10 mg, are tested in dynamic conditions (i.e. without any temperature plateau) up to 800 °C, at a slow heating rate of 4 °C/min.

Scanning Electron Microscopy (SEM) observations with the secondary electron (SE) and backscattered electron (BSE) detectors, are coupled to Energy Dispersive Spectroscopy (EDS) for chemical element analysis. Chalk samples are observed either along a fracture surface, or after epoxy resin impregnation, as in [20]. In the latter case, polishing is performed until a mirror-like surface is obtained, by using rotating disk tissues deposited with 1µm-size diamond particles. Ethanol is used as a lubricant for polishing purposes, to avoid interactions with water.

FIB/SEM analysis provides 3D images of the microstructure, without any preliminary preparation (and damage) of the observed surface. To this purpose, the chalk sample is finely polished (down to mirror-like finish). The focused ion beam (FIB) cuts a U-shaped hole in order to isolate a plane-parallel chalk volume [21]. The plane-parallel chalk volume is then covered with a platinum coating, in order to provide adequate electrical conductivity to the sample. This also allows maximum contrast with the observed surface. Following this, the FIB cuts regularly spaced 50 nm thick slices from the plane-parallel volume, perpendicularly to the sample polished surface. Between each FIB cutting, the chalk matter perpendicular to the polished surface is observed with an electron detector of the *in lens* type, which detects both secondary and backscattered electrons. This provides an image reflecting both the sample roughness (thanks to the SE) and its chemical composition (the image contrast is given by the BSE). Dozens of images have been taken on a chalk sample in the initial reference dry state.

Argon gas permeability under hydrostatic loading is a measurement of chalk ability to be flown through by a fluid, see details in Section 2.2.4.

*2D image analysis for pore network assessment*. 2D image analysis is performed on a number of SEM/BSE images of resin-impregnated and polished chalk, using Java programming and the free software ImageJ (see http://rsb.info.nih.gov/ij/). The aim is to assess (1) chalk porosity and (2) its pore size distribution using standard image analysis techniques. Comparison of results is made

between a reference dry sample (Sample 1) and a sample heat-treated at 500 °C for 48 h (Sample 2). For Sample 1, 14 SEM/BSE images are used at resolutions ranging from 0.033µm/pixel to 1.667µm/pixel; for Sample 2, 57 SEM/BSE images are used within an identical resolution range, see Table 1.

Table 1. Number of SEM/BSE images used per resolution, and per sample.

| **Resolution (µm/pixel)** | **Sample 1** | **Sample 2** |
|---|---|---|
| 1.667 | 1 | 3 |
| 1.111 | None | 1 |
| 1.0 | 3 | 4 |
| 0.833 | 1 | None |
| 0.5 | 1 | None |
| 0.4 | 1 | 3 |
| 0.333 | 1 | None |
| 0.25 | 1 | 4 |
| 0.167 | 1 | 5 |
| 0.143 | 1 | 1 |
| 0.1 | 2 | 24 |
| 0.033 | 1 | 12 |
| Total | 14 | 57 |

Each image is processed as follows. First, the bottom caption is removed and the grey level histogram is shifted in order to span the whole 256 possible grey levels (in 8-bit format). Secondly, five different thresholding techniques, available as standard in ImageJ, have been used to segment solid matrix (in white) and pore network (in black): the result is a binary image, ready for porosity and pore size distribution analysis. The five segmentation (or binarization) techniques are: Kapur–Sahoo–Wong method (also called the Maximum Entropy method) [22], the IsoData algorithm [23], which is proposed as the default binarization method, the Moments method [24], Otsu algorithm [25] and Huang fuzzy thresholding algorithm [26]. After binarization, and without further morphological operation, porosity is assessed as the ratio between the number of pixels corresponding to the pores (black pixels) and the total number of pixels of the image. When several images are available, average porosity and standard deviation are calculated.

For pore size distribution assessment, isolated pixels are removed in order to avoid noise effects: these are either the smallest pores in the lower detection range of the SEM, or image artifacts. To do so, morphological operations are performed, as follows: each image is subjected to a series of closing operations, namely a series of dilations followed by erosion, the intensity varying with resolution. The algorithm analyses the eight neighboring pixels of one given pixel. If dilation intensity is set to one, then, for a white pixel, it is sufficient that one of its eight neighboring pixels be white to set the whole eight pixels to white (i.e. to solid): this is the maximal intensity available. The rule is symmetrical for a black pixel. On the opposite, if dilation intensity is set to $1 < n \leq 8$, the eight pixels around a given white pixel are set to white (solid) whenever it has at least $n$ white pixels among its neighboring pixels. Moreover, closing intensity depends on two different parameters: the number $n$ of selected neighboring pixels for the dilation/erosion, as discussed

previously, and also the number of iterations of the dilation/erosion process. Setting these parameters correctly is the key to this analysis. Indeed, if the dilation/erosion intensity is too high for a low resolution image, smaller pores may be suppressed from the evaluation. Favoring closing operations over opening ones (i.e. dilation followed by erosion instead of erosion followed by dilation) is bound to affect our results. This will be the subject of further work. By visual analysis, parameters are fixed at $n$=5 pixels at a resolution of 0.033µm/pixel, $n$=7 pixels at a resolution of 0.1µm/pixel and $n$=8 pixels at a resolution of 0.167µm/pixel, each iterated four times.

After the closing iterations, each image is subjected to two distinct calculations, which both provide a pore size distribution. Voronoi tessellation algorithm calculates the pore network skeleton, so that each pixel of this skeleton has a grey level equal to the local distance (in pixels) to the pore walls. The grey level histogram of Voronoi tessellation provides a pore size distribution. This method is adapted to well-connected porosity. For isolated pores, often present in a 2D image, the binary image is rather transformed by a watershed algorithm: the pore network is eroded until reaching its nodes, which are then dilated until a partition line is identified between neighboring particles. ImageJ identifies these particles as ellipses and provides the distribution of their small and great axis. Whenever actual particles are more rectangular than elliptic, as in Haubourdin chalk, a correction, by a factor of $\sqrt{\pi}/2$ to the axis values, is used to derive the length and width of the particles, see [27].

### 2.2.2. Uniaxial compressive tests

Mechanical performance of Haubourdin chalk is compared in the initial reference dry state, after partial water saturation and after heat treatment, by performing uniaxial compressive tests up to sample failure, as follows.

Four strain gauges are glued on each sample surface, in the mid-height plane and at an angle of 90° with respect to the other: two are longitudinal (and at an angle of 180°), and two are transversal (at an angle of 180°). After heat treatment, and prior to strain gauge placement, each sample is covered with an impermeable polymer coating in order to avoid water intake (or loss) from surrounding air humidity, to which chalk is particularly sensitive, see [3]. No such coating is used for reference dry samples. Uniaxial compressive load is imposed by a Zwick$^{TM}$ mechanical machine equipped with a load cell ranging up to 250.000 kN±0.005. This provides an accuracy of ±0.0046 MPa for a 37 mm diameter sample. Compression platens are mounted to the machine with a ball-joint to avoid bending moments on the sample.

Each test is performed at a constant displacement rate of 2µm/s with loading/unloading cycles up to sample failure. Young's modulus $E$ is assessed during three loading/unloading cycles from 2 MPa and up to 4 MPa, in order to remain in the initial linear elastic domain. Uniaxial compressive strength $f_c$ is taken as the peak normalized stress achieved by each sample.

### 2.2.3. Hydrostatic compressive tests: drained and undrained conditions

Mechanical performance of Haubourdin chalk is also compared in the initial reference dry state, after partial water saturation and after heat treatment, by performing hydrostatic compressive tests, mainly in drained conditions, i.e. here, with zero relative pore pressure [28]. As detailed in Section 2.2.2, a chalk sample is equipped with four strain gauges, which provide each a strain value noted $\varepsilon_1$, $\varepsilon_2$, $\varepsilon_3$ and $\varepsilon_4$. It is then placed in the triaxial cell, which imposes a given hydrostatic stress (or

confinement) $P_c$. Under given confinement, the volumetric strain εv is deduced with an assumption of isotropy, as $\varepsilon_v=3\times(\varepsilon_1+\varepsilon_2+\varepsilon_3+\varepsilon_4)/4$.

In drained conditions (zero pore pressure), with an assumption of linear elasticity, the elastic drained bulk modulus $K_b$ relates hydrostatic stress variation $\Delta P_c$ and volumetric strain variation $\Delta\varepsilon_{v1}$, as follows [28], [29]:

(1) $$\Delta P_c = - K_b \, \Delta\varepsilon_{v1}$$

where $_{\Delta PC}$ is counted positive in compression. Drained triaxial tests are conducted by monotonically increasing $P_c$ up to 30–50 MPa, until pore collapse. This corresponds to a significant decrease in *tangent* elastic drained bulk modulus $K_b$ (when compared with its initial value) and also to irreversible strains, see [3], [8]. Yet, despite the chosen loading mode (monotonously increasing), no assessment of $K_b$ during a linear elastic unloading phase is undertaken, so that only its initial value (corresponding to the sole linear elastic behavior phase of the tests) is measured.

Our aim is to compare the effect of different heat-treatment temperatures, and that of partial water-saturation on $K_b$ values and on pore collapse. Pore collapse stress is taken as equal to the yield stress, i.e. to the upper limit in hydrostatic stress of the initial linear elastic behavior domain. The seven samples tested in drained triaxial compression are in the following conditions: one sample is in the reference dry state, one after 105 °C heat-treatment, one after 300 °C heat-treatment, two after 500 °C heat-treatment, one at 30% water saturation level and a final one at 80% water saturation level.

Due to the difficulty in performing undrained experiments, the latter conducted on two different samples only, one after 60 °C oven-drying and the other after 500 °C heat-treatment. The interstitial pore pressure $P_i$ is slowly increased at given confinement $P_c$. $P_i$ and $P_c$ values are kept below 20 MPa, in order to remain in the linear elastic domain. At given $P_c$, each pore pressure variation $\Delta P_i$ induces a volumetric strain variation $\Delta\varepsilon_{v2}$, so that the following relationship may be identified by linear interpolation:

(2) $$\Delta P_i = H \, \Delta\varepsilon_{v2}$$

Along a single monotonously increasing stress path, the solid matrix bulk modulus $K_s$ is then derived from $K_b$ and $H$ as [29], [28]

(3) $$1/K_s = 1/K_b - 1/H$$

Nur and Byerlee [30] have shown that the Biot coefficient may be deduced from

(4) $$b = 1 - K_b / K_s$$

### 2.2.4. Measurement of gas permeability and/or pore volume variation under confinement

The experiments described in this section are performed in a temperature-controlled room, at 20–22 °C, in order to limit any thermally induced variation of measured properties.

Gas permeability tests are performed in the initial reference dry state (after 60 °C oven-drying) by a quasi-static flow method using argon gas, and by assuming the perfect gas law [31], [32]. Two different samples are tested by this method. Each chalk sample is placed in the triaxial cell, see [32] for further details on the set-up. This enables the sample to be subjected to a hydrostatic stress (or confinement) of 4 MPa, which is assumed to be sufficiently low not to induce any significant

damage, and sufficiently high to close up any existing micro-crack. A 200 ml buffer reservoir is plugged on the sample upstream side in order to ensure that the sample is subjected to a stable gas pressure value. At a given upstream gas injection pressure of 1.42 MPa, effective gas permeability is measured during a small decrease in upstream gas pressure by 0.4 MPa.

For the coupled experiment providing effective gas permeability and porosity variation, a reference dry sample of Haubourdin chalk is placed in the triaxial cell, as for gas permeability measurements. Confinement is gradually increased from 1 to 60 MPa, and then decreased down to 1 MPa. Simultaneously, a dedicated gas panel is plugged to the sample upstream and downstream sides, in order to assess both its effective gas permeability and its pore volume variation at each given confinement value.

For gas permeability measurement, a buffer reservoir with a calibrated volume of 420 ml is connected to the sample upstream side; it is placed initially at a 0.5 MPa relative pressure value, while the downstream side is at atmospheric pressure (i.e. zero relative pressure).

To measure pore volume variation, a buffer reservoir with a calibrated volume $V_1$ of 140 ml is connected on the sample downstream side, while the upstream buffer reservoir is isolated from the circuit by closing another valve. Before the actual test, the dead volume $V_2$ of the gas pipes between the downstream buffer reservoir and the sample is measured by placing a non-porous sample (made of steel) inside the triaxial cell, and by using the same procedure as follows. Initially, the sample is isolated from the argon gas panel by closing two valves (one at each sample end). The downstream buffer reservoir is placed at a pressure $P_{ini}$ of 0.4 MPa, measured by a manometer with a relative accuracy of 0.04% of its whole 0.1–0.4 MPa range. The valve connecting the buffer reservoir and the sample is then opened, and the new gas pressure $P_{end}$, recorded at stabilization, corresponds to a volume equal to $V_1+V_2+V_p$, where $V_p$ is the sample pore volume. The perfect gas law, applied to argon, provides $V_p$ by the following relationship:

(5) $$V_1 P_{ini} = (V_1 + V_2 + V_p)\ P_{end}$$

Finally, the total accessible Lagrangian porosity is given by $\phi = V_p / V_0$, where $V_0$ is the initial total sample volume. For the porosity and sample dimension range of Haubourdin chalk, the absolute accuracy of $\phi$ measurement is of 0.2%. This procedure is repeated at each given confinement value. It is presented in more detail in [33].

# 3. Results

## 3.1. Initial microstructure, hydraulic and mechanical behaviour

Prior to investigating the effect of water and heat-treatment on Haubourdin chalk performance, results for its initial reference dry state are presented, in terms of microstructural features, hydraulic and mechanical performance. These will be of key importance when comparing performance with water-saturated or heat-treated chalk.

### 3.1.1. Main microstructural and hydraulic features

*Basic microstructure parameters*: Mineralogical analysis using Bernard calcimetry highlights the high purity of Haubourdin chalk, which is made on average of 98% $CaCO_3$±1. The non-soluble 2% part of Haubourdin chalk is identified by XRD experiments: it is made of 95% montmorillonite, which is a swelling smectite clay, and 5% illite, with traces of quartz.

Based on the ethanol saturation method, the basic characteristics of reference dry Haubourdin chalk are as follows: (1) its total connected porosity $\phi$ has an average value of 40.1%±0.6, (2) its apparent dry density is on average 1.57 g/cm$^3$±0.03, and (3) its solid dry density (or grain density) is on average 2.60 g/cm$^3$±0.01. These properties display a very limited variability, measured on 10 different samples: it is attributed to the high mineralogical purity of Haubourdin chalk, see above. This also means that different sample sizes do not affect porosity results significantly. Nevertheless, the value for solid dry density (2.60 g/cm$^3$±0.01) for an almost pure chalk (98% $CaCO_3$) such as Haubourdin appears relatively low when compared to usual values for pure calcite (more on the order of 2.71 g/cm$^3$), see for instance [10] and Table 6. Actually, a difference of 0.11 g/cm$^3$ compared to a reference value of 2.71 g/cm$^3$ represents 4% of this value only. As a matter of comparison, helium pycnometry provides an average solid dry density of 2.77 g/cm$^3$ with a standard deviation of 0.03 g/cm$^3$, which is closer to the expected values, with a difference representing 2.2% of the reference 2.71 g/cm$^3$ value. Therefore, it is thought that ethanol has possibly not saturated all pores of the chalk, yet to a very limited extent. The ethanol saturation method rather provides lower bound values for density, and, as will be shown below, for porosity too.

As a matter of comparison, MIP provides an average value for porosity at 42.0%±0.8, see Table 2. Bulk density (i.e. apparent dry density) is given at 1.695 g/cm$^3$±0.02 and skeletal density (i.e. solid grain density) is at 2.92 g/cm$^3$±0.07. All three values are greater than those obtained by ethanol saturation. Solid grain density is significantly higher (by 8%) than that usually measured for pure calcite (at 2.71 g/cm$^3$, see [10] and Table 6) and than that given by helium pycnometry for this chalk (2.77 g/cm$^3$±0.03). These results are attributed to elevated mercury pressures (up to 200 MPa), which enter more pore space, or even break some elements of the solid skeleton of chalk, hence increasing measured porosity and solid density. From MIP results, see also Table 2, total pore area, i.e. surface specific area, is on average 2.00 m$^2$/g±0.15, which is consistent with usual values for chalk, see [10]. As Heggheim et al. [10] state, this is almost 10 times larger than for pure sandstone rocks (without significant clay amounts), and it is indicative of an open microstructure, with large porosity. Depending on the measurement method used during MIP data analysis, the median pore diameter ranges between 0.469µm and 0.711µm, while the average pore diameter is of 0.497µm±0.03. These data will be compared with 2D image analysis of SEM observations of Haubourdin chalk, see below.

Table 2. Full set of Mercury Intrusion Porosimetry (MIP) results, for two different chalk samples C1 and C2, after 60 °C drying, and before heat treatment.

| | **Sample C1** | **Sample C2** |
|---|---|---|
| Total intrusion volume (ml/g) | 0.246 | 0.249 |
| Total pore area ($m^2$/g) | 1.867 | 2.137 |
| Median pore diameter (from volume) (μm) | 0.711 | 0.701 |
| Median pore diameter (from area) (μm) | 0.575 | 0.469 |
| Average pore diameter (from 4V/A) (μm) | 0.528 | 0.466 |
| Bulk density at 0.10 psia (g/ml) | 1.674 | 1.717 |
| Apparent (skeletal) density (g/ml) | 2.85 | 3.00 |
| Porosity (%) | 41.2 | 42.8 |

To conclude, with such basic microstructure characteristics, Haubourdin chalk is placed within the range of medium density material [16], and high porosity chalk [10].

*Basic hydraulic properties*: For 60 °C oven-dried chalk subjected to $P_c$=4 MPa, the effective gas permeability is $2.0\times10^{-15}$ $m^2$±0.1 (or $2.0\times10^{-8}$ m/s±0.1), i.e. 2.0 mD±0.1. For chalks, such value is typical and it is considered a low value [10]. It is associated with a high average porosity (of 42.0% ±0.8, given by MIP). The data for Liège chalk ($\phi$=40–43% and $K$=1–2 mD) and Danish Stevns Klint chalk ($\phi$=45–52% and $K$=3–5 mD) are very similar. These chalks are from the same sedimentary basin as Haubourdin chalk [34], and they have a very high $CaCO_3$ content: 98% for Liège chalk and 96% for Stevns Klint chalk, similarly to Haubourdin chalk (with 98% $CaCO_3$).

*Detailed microstructural features*: Let us now analyze the microstructure arrangement of Haubourdin chalk. On a qualitative level, SEM analysis of resin-impregnated and polished samples shows that Haubourdin chalk may be considered as a Wackestone, according to the Dunham classification [35], [6], [5], see Fig. 3(a) and (b): it is supported by a calcite mud (made of individual small calcitic particles), and contains generally more than 10% grains (which may be calcitic grains or micro-fossils), and less than 90% mud. Micro-fossils are mainly foraminifera and calcispheres with diameters up to 100μm, such as in [36]. This classification is also that of French St Marguerite s/Mer and Hardivilliers chalks, whereas Précy-sur-Oise and Belgian Obourg chalks are Mudstones, see [6]. French Beauval chalk is a mix of Mudstone, Wackestone and Packstone [6].

By observing failure surfaces more closely, it can be seen that Haubourdin chalk is made up of various micro-fossils and more or less decomposed coccolith disks with diameters of up to 5μm, see Fig. 2. Coccolith disks decompose as calcitic grains (or bricks), with an average size of about 2–3μm: these make up the so-called calcitic mud, which mainly supports external loads. It is the extent of the cementation between these grains, which provides coherence to the solid skeleton, and this contributes primarily to chalk mechanical strength. Without extensive grain cementation, chalk is mainly sustained by grain interlocking, as provided by mechanical compaction and calcite re-crystallisation during diagenesis [2], [6]. Besides coccolith disks and calcitic bricks, a few angular calcite crystals are observed, see Fig. 2, which hint at possible (though minor) calcite re-crystallisation and grain cementation. In impregnated and polished samples, low porosity aggregates of calcite also appear, with a shape similar neither to that of a coccolith fragment nor to that of a micro-fossil. As proposed by Hjuler et al. [6], these low porosity aggregates are interpreted as calcite precipitations caused by meteoric diagenesis. These heavily overgrown aggregates are

situated in relatively unaltered calcite mud matrix, so that they correspond to a different calcite redistribution mechanism (in ground water) than the homogeneous recrystallisation and cementation processes, which are observed in deeply buried chalks.

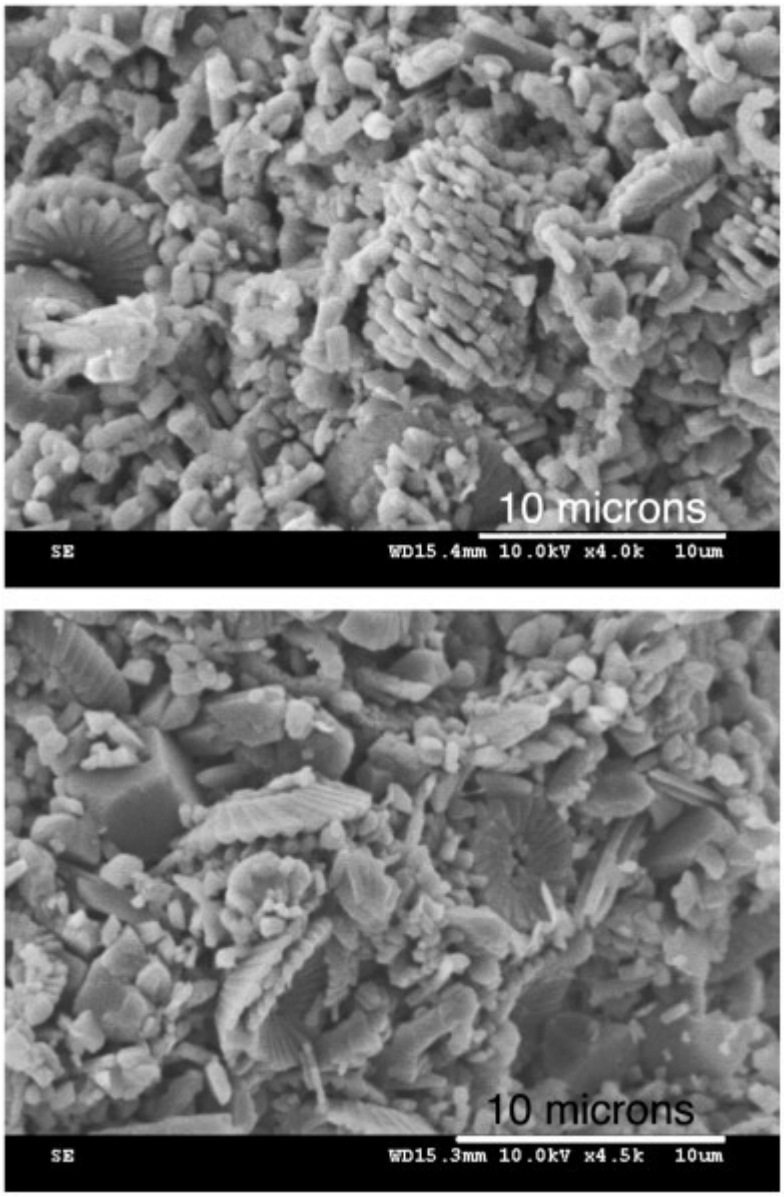


Fig. 2. Observations of 60 °C oven-dried chalk without epoxy resin impregnation, using the SEM/SE detector. These show entire coccolith disks, and (center of top image) the imbrication between calcite grains (which constitute the coccoliths), or (top left of bottom image) several angular calcite crystals, for which chemical composition is proven by EDS analysis.

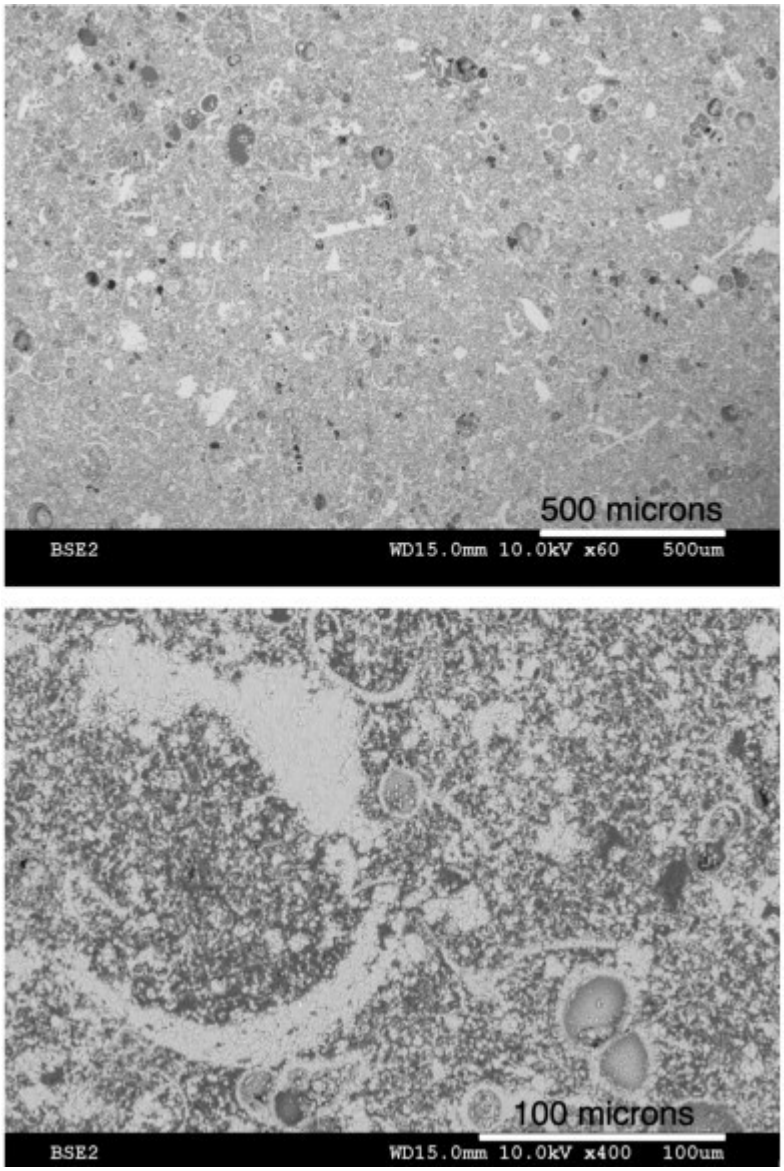


Fig. 3. SEM observations of Haubourdin chalk after epoxy resin impregnation and polishing, using the BSE detector after 60 °C oven-drying.

To complete this microstructure analysis, entire, undamaged, coccospheres have been observed by FIB/SEM, highlighting the very limited diagenesis processes (i.e. compaction, recrystallisation or cementation) sustained by this chalk, see Fig. 4. Initially, these images obtained by FIB/SEM should have been transformed to a binary format, so that a 3D pore network would have been reconstructed and analyzed quantitatively. This was not possible with this particular image series, due to thresholding difficulties in presence of a strong greyscale background (calcitic grains inside the pores of each sectioning plane are too visible, and bias the thresholding). This will be improved in further work. To conclude, Haubourdin chalk may be classified according to Hjuler et al. repartition [6], as an outcrop chalk subjected to shallow burial.

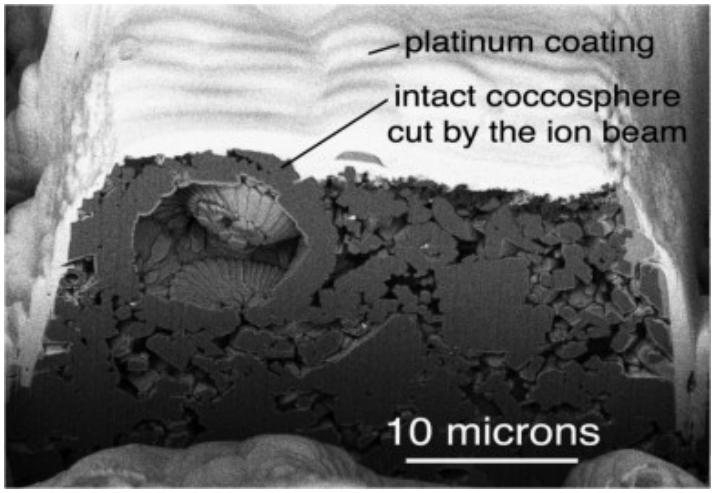


Fig. 4. Observations of 60 °C oven-dried chalk without epoxy resin impregnation, using the FIB/SEM apparatus showing the presence of a full coccosphere, which indicates very limited compaction.

*2D image analysis for porosity and pore size distributions*: Porosity has been assessed from 2D analysis of SEM images in the reference dry state (Sample 1), see Fig. 3(a) and (b), and after heat-treatment at 500 °C for 48 h (Sample 2), see Fig. 5(a) and (b).

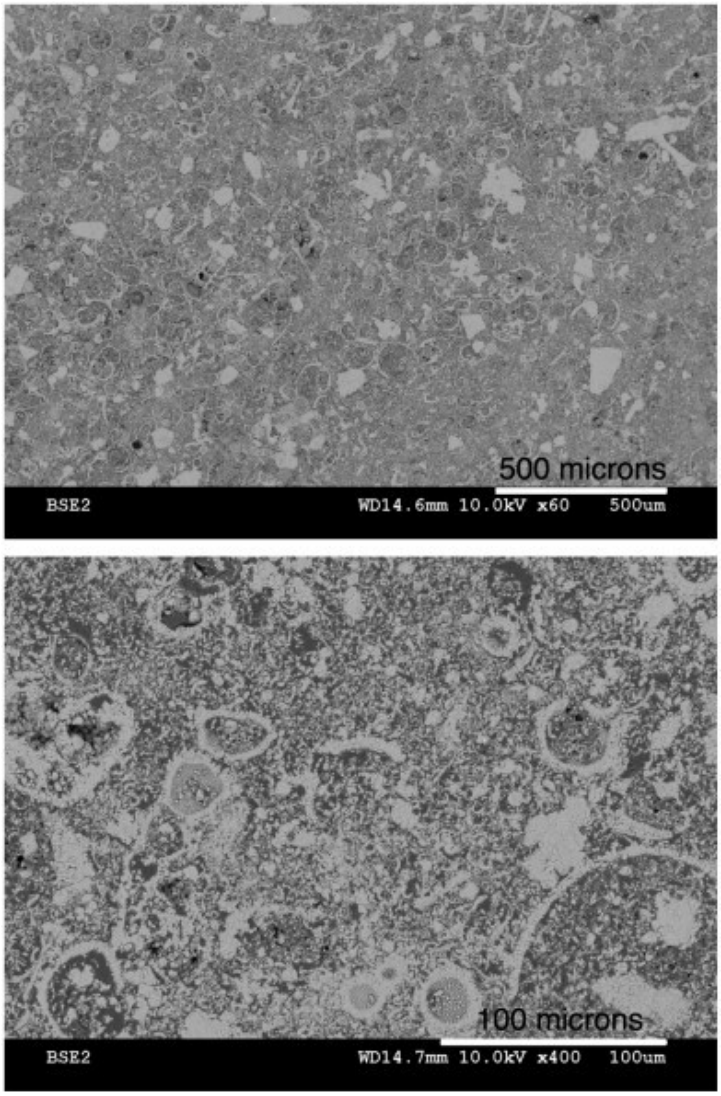


Fig. 5. SEM observations of Haubourdin chalk after epoxy resin impregnation and polishing, using the BSE detector after 500 °C heat-treatment for 48 h.

Porosity of reference dry chalk is very close to MIP ($\phi$=42.0%±0.8), when estimated by 2D image analysis for resolutions down to 0.1µm/pixel. For instance, at 0.1µm/pixel, with the Maximum Entropy Algorithm, $\phi$ is on average 42.3% with a standard deviation of 0.1. Nevertheless, depending on the thresholding method, $\phi$ may go up to 45.7% (standard deviation of 1.1), obtained with the Huang algorithm. Such non-negligible standard deviation value is attributed to the limited number of images available for this assessment. At lower resolution, $\phi$ is over-estimated, because the image are no longer sufficiently representative of the microstructure.

For 500 °C heat-treated chalk, a greater number of images are used. It is shown that image analysis provides consistent values whatever the segmentation algorithm, provided that image resolution is at least half (or rather, one order of magnitude) lower than the microstructure characteristic size, which is on the order of 1µm for Haubourdin chalk. For instance, at 1.67µm/pixel, with Huang algorithm, $\phi$ is above 62%, whereas $\phi$ is as low as 30.1% with the Maximum Entropy algorithm. At 0.033µm/pixel, several images comprise mainly calcitic aggregates, which biases the assessment. With these precautions in mind, it is shown that, similarly to reference dry chalk, $\phi$ is slightly over-estimated when compared mainly with MIP. At 0.1 and 0.167µm/pixel, $\phi$ is on average, respectively, 43.9% (with a standard deviation of 0.4) and 43.5% (with a standard deviation of 0.9). Finally, when comparing $\phi$ for both samples 1 and 2, it is concluded that a 48 h heat-treatment at 500 °C does not significantly modify chalk porosity (Fig. 6).

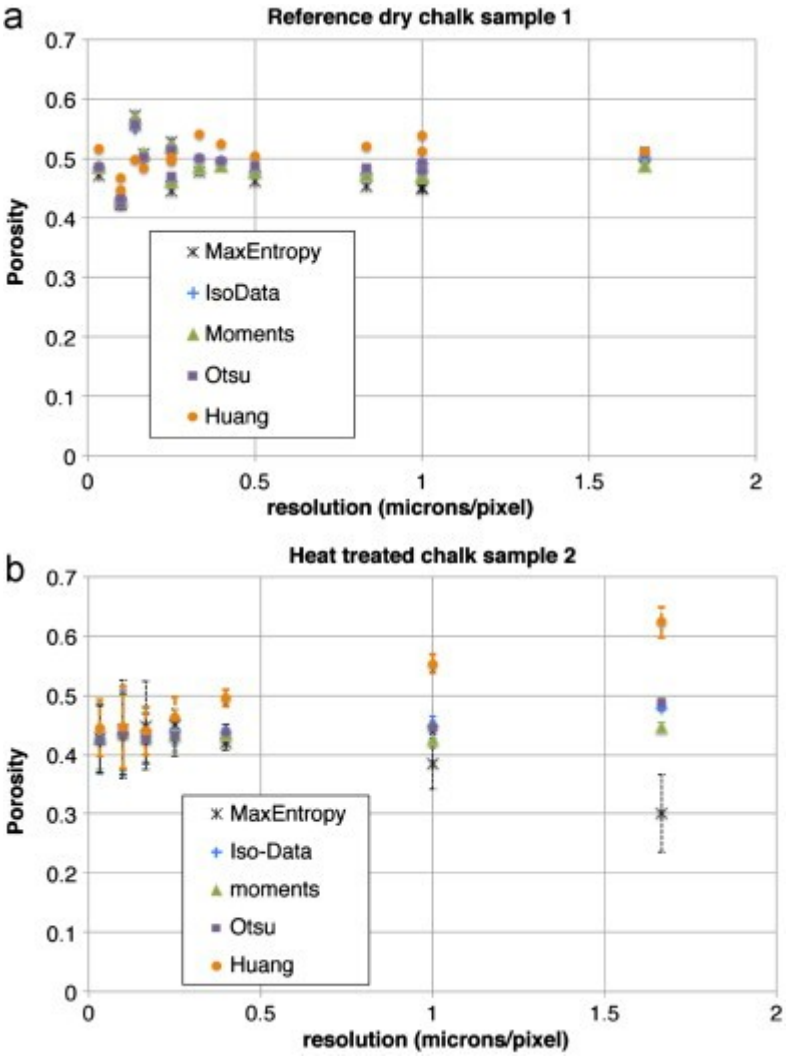


Fig. 6. Porosity assessment using 2D image analysis from SEM observations (a) before heat treatment; (b) after heat treatment up to 500 °C for 48 h.

Pore size distribution data, obtained by 2D image analysis, are compared to the results of MIP, for different image resolutions, from 0.167µm/pixel down to 0.033µm/pixel, see Fig. 7. In this figure, at each given image resolution, the total sum of volumetric fractions (calculated on each pore size interval [r; r+image resolution]) is taken as equal to one. Results show that the peak pore size is predicted at a value of 0.854µm by MIP, and it is well reproduced by both the Voronoi and watershed methods. For instance, at 0.033µm/pixel, the Voronoi method gives a peak pore size of 0.866µm, and the watershed method gives 0.856µm, which is very close to MIP. Overall, pore size distributions given by image analysis are more widely spread than those obtained by MIP: distributions obtained by image analysis predict a greater number of pores, which are bigger than the peak pore size than by MIP. This is not attributed to the bias due to the 2D technique, which cannot assess actual pore sizes as a 3D image would allow. Indeed, for both porosity and peak pore size, 2D image analysis provides satisfactory assessment, in good agreement with MIP results. Instead, image analysis does not depend on liquid intrusion through pores of varying throat sizes, as MIP does [37], so that smaller pores are accounted for by the former.

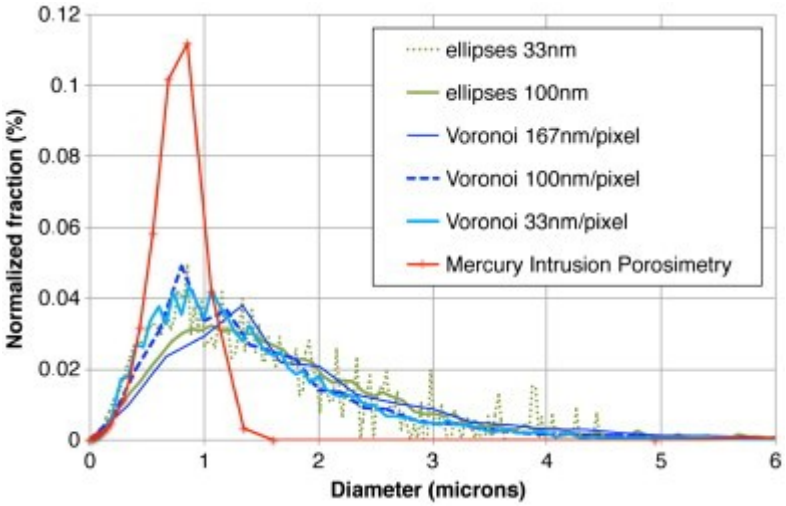


Fig. 7. Pore size distributions obtained by Mercury Intrusion Porosimetry (MIP) on a reference dry sample, and 2D image analysis on chalk sample 2, after 48 h heat treatment at 500 °C.

### 3.1.2. Mechanical performance

Using all of the 15 reference dry samples tested in this study, and without analyzing sample orientation (and possible anisotropic effects), uniaxial compressive strength $f_c$ of Haubourdin chalk is of 14.7 MPa±1.5, with a standard deviation of 1.9 MPa, which represents 12.9% of the average. For each sample tested, failure planes are along the load axis, which is typical of a failure in tension. A similar failure pattern is observed for weak Lewes Normandy chalk (from Bois-de-Cise, France), see [38] and Table 7. Also, the initial Young modulus $E$ of Haubourdin chalk is 10.0 GPa on average, with a standard deviation of 1.95 GPa, which represents 19.5% of the average. This significant scatter is attributed to chalk anisotropy, see below. The Poisson ratio has been assessed for only two samples, with values of 0.2 and 0.21.

*Haubourdin chalk anisotropy*: Chalk anisotropy has been assessed for six samples, in which sampling direction is known, see Table 3. Average uniaxial strength $f_c$ is slightly greater for vertical chalk samples than for horizontal ones, with an average of 16.45 MPa (and standard deviation of 1.28), compared to 14.2 MPa (standard deviation of 1.06) for horizontal samples. This difference in $f_c$ is attributed to chalk anisotropy [39], yet it remains relatively limited, so that it will not be taken

into account in further work. For the Young modulus *E*, although the average is greater for vertical samples than for horizontal ones (11,010 MPa and 10,020 MPa, respectively), the results overlap, with values ranging from 9770 to 11,470 MPa for vertical samples, and from 9440 to 10,740 MPa for horizontal samples. Based on these tests, Haubourdin chalk is anisotropic (at least transverse isotropic), if to a limited extent.

Table 3. Uniaxial compressive test results for vertically or horizontally cored Haubourdin chalk samples.

| **Sample no. (horizontal coring)** | **Uniaxial strength $f_c$ (MPa)** | **Young's modulus *E* (MPa)** |
|---|---|---|
| 1 | 12.98 | 9880 |
| 2 | 14.93 | 9440 |
| 3 | 14.68 | 10,740 |
| | | |
| Average | 14.2 | 10,020 |
| Standard deviation | 1.06 | 660 |

| **Sample no. (vertical coring)** | **Uniaxial strength $f_c$ (MPa)** | **Young's modulus *E* (MPa)** |
|---|---|---|
| 1 | 16.94 | 11,470 |
| 2 | 15.0 | 11,800 |
| 3 | 17.42 | 9770 |
| | | |
| Average | 16.45 | 11,010 |
| Standard deviation | 1.28 | 1090 |

## 3.2. Effect of partial water saturation

As clearly shown in the literatures [3], [4], [8], [9], [10], [38], [39], [40], [41], chalk strength decreases significantly whenever chalk is partially water-saturated: this is the so-called *water-weakening effect*. For Haubourdin chalk, it is readily seen on a stress–strain curve, when comparing dry and fully water-saturated samples, see Fig. 8. Dry chalk has a brittle linear elastic behavior until peak strength, whereas water-saturated chalk has a non-linear plastic behavior up to its peak strength. For these single tests, peak strength decreases by 1.75 MPa from dry to fully water-saturated chalk, i.e. it decreases by 43%.

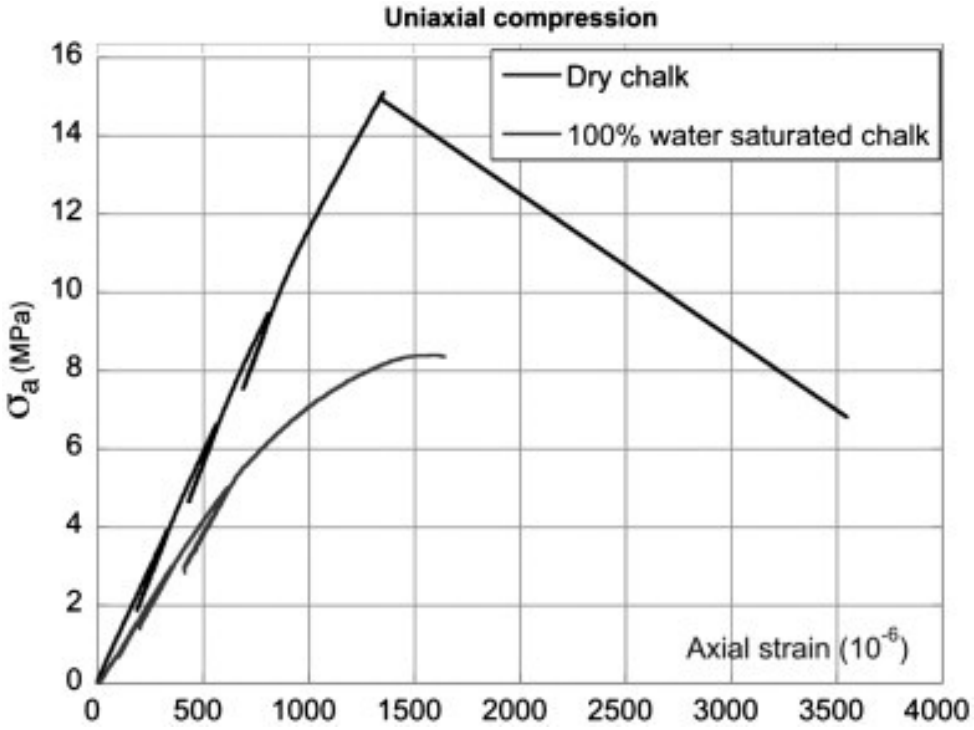


Fig. 8. Stress–strain curves for chalk samples under uniaxial compression, either dry (after oven-drying at 60 °C) or 100% water saturated.

For our whole dataset, the decrease in $f_c$ and $E$ has been quantified as a function of water saturation level $S_w$, see Fig. 9. From as low as $S_w$=1% saturation, $f_c$ decreases by 23.8% when compared to the dry reference state, and $E$ decreases by 19%. The decrease in strength and Young's modulus reaches an asymptote at as low a saturation as $S_w$ =3%, with a decrease in $f_c$ by 42.8% and a decrease in $E$ by 21%. At $S_w$=22% saturation, there is a 41.5% decrease in $f_c$ (with a value of 8.6 MPa, result from one single sample); for $E$, the decrease at $S_w$=22% is of 24% (with $E$=7600 MPa, result for one single sample). At $S_w$=100% saturation, the average decrease in $f_c$ is of 44.8% (with an average value of 8.36 MPa, calculated on 10 different samples); for $E$, the decrease at $S_w$=100% is of 15% (with $E$=8450 MPa, result for one single sample).

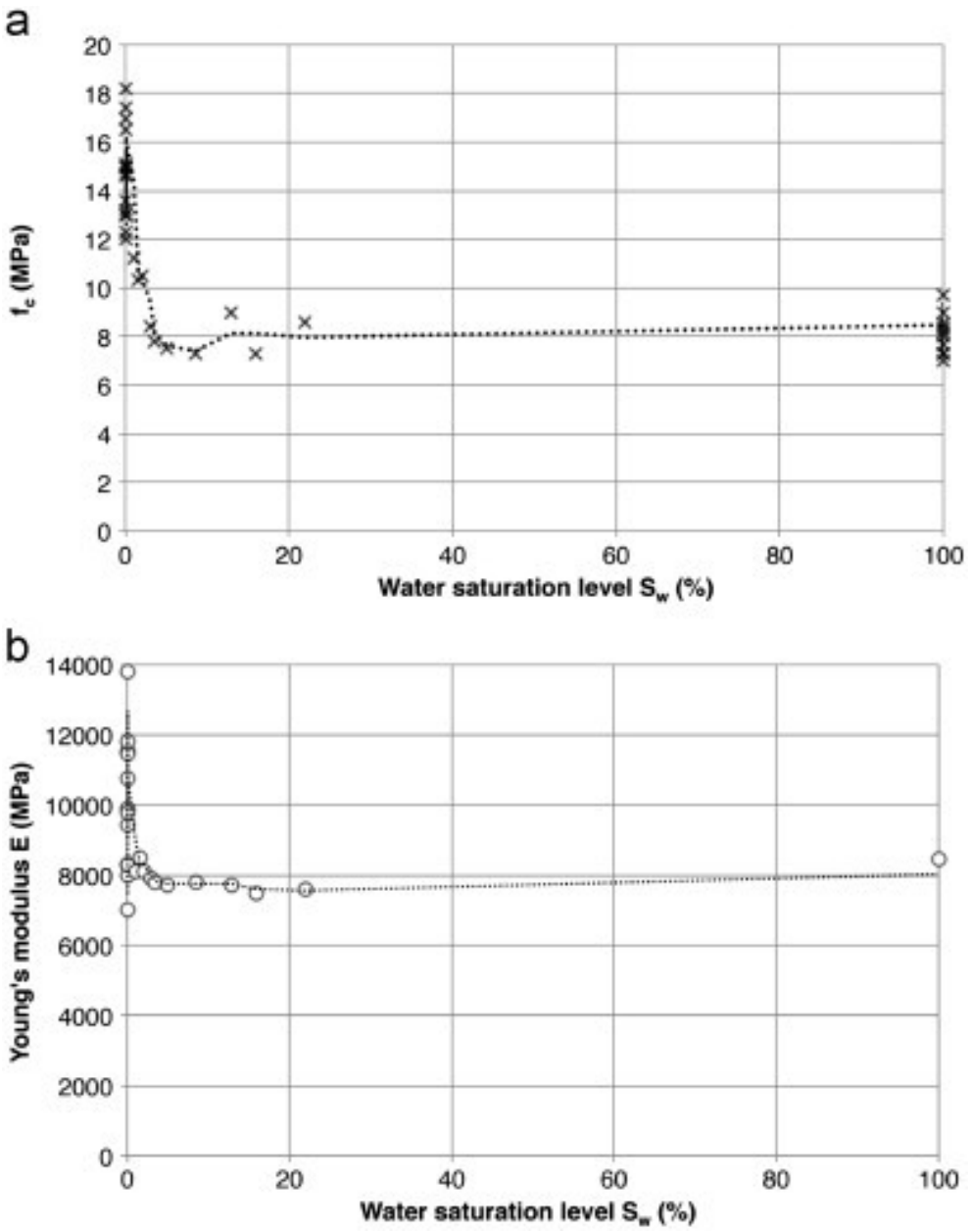


Fig. 9. (a) Uniaxial compressive strength $f_c$ and (b) Young's modulus $E$ with increasing water saturation level $S_w$, for values up to 22%.

Such amplitude in the decrease of strength and Young's modulus is typical for chalks, see [38], [42]: for Upper Yorkshire chalk, $f_c$ decreases from an average of 25.6 MPa in the dry state to an average of 11.9 MPa in the fully water-saturated state, i.e. it decreases by 53.5%. Middle Norfolk chalk displays a strength decrease from an average of 13.0 MPa in the dry state to an average of 5.8 MPa in the fully water-saturated state, i.e. it decreases by 55.4%. The uniaxial compressive strength of French Lewes chalk decreases from 4 MPa (dry state) down to 0.84 MPa at a water content $w$ of 18%, i.e. it decreases by 79%, see [38].

*Effect of varying water imbibition*: The length of time during which chalk is placed at 100% water saturation may affect its strength properties. This was tested for imbibition durations ranging between 8 and 65 days, see Fig. 10. Values at zero imbibition time correspond to the reference dry state.

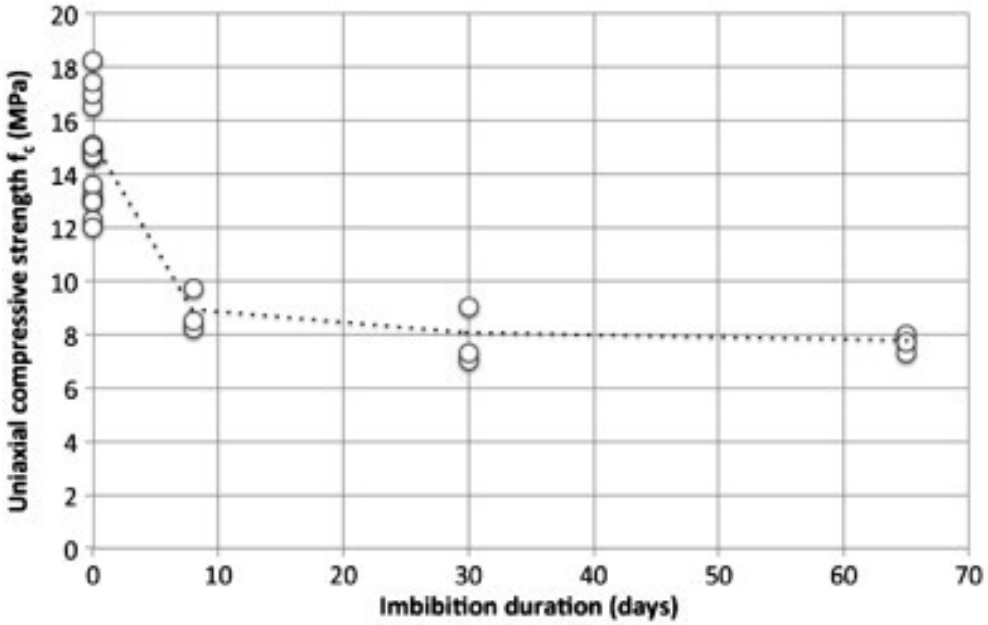


Fig. 10. Effect of time spent under water upon uniaxial compressive strength $f_c$.

It is observed that after 8 days under water, from which sample masses are stable, $f_c$ has reached an average of 8.8 MPa: it varies within a range of [8.2; 9.7] MPa. Subsequent durations under water imply a less noticeable decrease in $f_c$: $f_c$ is on average 7.8 MPa at 30 days (within a range of values of [7.0; 9.0] MPa), and 7.7 MPa at 65 days (within a range of values of [7.3; 8.0] MPa). All intervals (i.e. range of values) of these test results overlap, despite a monotonous decrease in the average $f_c$ value. More precisely, the initial loss in uniaxial compressive strength $f_c$, measured at 8 days, represents 40.1% of the average $f_c$ in the reference dry state; at 30 days, the loss in $f_c$ represents 46.9% of $f_c$ in the dry state; at 65 days, the loss in $f_c$ represents 47.6% of $f_c$ in the dry state. Therefore, the main decrease in $f_c$ is obtained after only 8 days under water, and it progresses then much more slowly, up to 65 days. It is concluded that, after 8 days, the duration of water imbibition has a more limited effect on chalk mechanical performance.

## 3.3. Effect of heat-treatment

By using Brazilian tensile tests on chalk, Madland [43] has investigated the effect of heat-treatment up to 250 °C: chalk strength increases by 25% after oven-drying at 250 °C, for a corresponding average weight loss of only 0.2% [40]. Although several authors claim a risk of thermal decomposition of the chalk [40], [44], the use of thermogravimetry analysis (TGA) shows that calcite decomposes into CaO and $CO_2$ above 600 °C only [13].

Therefore, we have investigated the effect of a heat-treatment up to 500 °C upon uniaxial compressive strength $f_c$, Young's modulus $E$ and Poisson's ratio ν, see Fig. 11. From an initial average strength $f_c$=14.7 MPa±1.5 in the reference dry state, $f_c$ remains stable up to 200 °C, with an average value of 14.6 MPa. $f_c$ increases significantly from 300 °C (with an average at 18.9 MPa at 300 °C) and up to 500 °C, with an average of 21.7 MPa. This represents a huge 47.6% increase of the average strength in the reference dry state. Heat-treatment for 48 h at 500 °C does not bring further strength improvement when compared with heat-treatment for 24 h at 500 °C. This is all the more so true as these samples were not protected against water intake from ambient air moisture, as other samples have been. From these results alone, it is concluded that heat-treatment provides an improvement of chalk mechanical strength, which makes it of interest to road building companies.

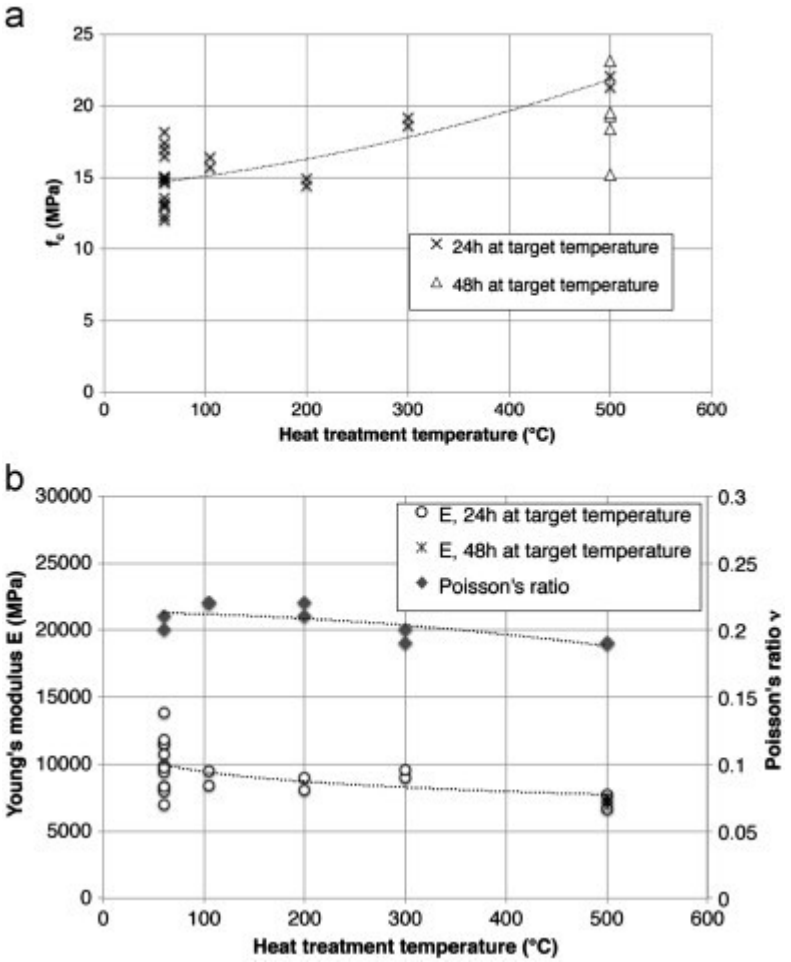


Fig. 11. (a) Uniaxial compressive strength $f_c$ and (b) Young's modulus $E$ and Poisson's ratio ν with increasing heat-treatment temperature $T$, for values up to 500 °C.

Besides, the Young modulus does not vary significantly above, or below, its range of values in the initial reference dry state, which is between 8.28 and 13.8 GPa, with an average at 10.0 GPa. Similarly, the Poisson ratio remains constant up to 200 °C, with a slightly lower value of 0.195 at 300 °C and 0.19 at 500 °C. This means that chalk rigidity is not significantly altered by heat-treatment.

*Effect of a limited water re-saturation*: As recalled by Risnes et al. [40], dry chalk is very hygroscopic and readily adsorbs moisture from the air. For instance, according to Schroeder [3], a chalk sample dried at a temperature slightly above 100 °C adsorbed water to a saturation of 0.85% within one and a half hours, and then remained at a relatively stable mass. This spontaneous re-saturation of chalk may induce a strength loss, despite the positive effect of heat-treatment.

To assess this experimentally for Haubourdin chalk, two samples have been heat-treated at different temperatures $T_{max}$, re-saturated at 1.5% and then tested for mechanical strength. Re-saturation is obtained at mass stabilization by using a salt saturated solution imposing a low 43% relative humidity in the atmosphere surrounding the samples, as in Section 3.2. Results are given in Table 4. It is observed that, as expected, Haubourdin chalk loses a significant proportion of the compressive strength gained by heat-treatment. In particular, 300 °C heat-treated chalk recovers its strength as in the initial reference dry state (after 60 °C oven-drying only), with a value $f_c$=14.5 MPa. After 500 °C heat-treatment, chalk retains a limited strength increase as compared to the initial reference dry state, with $f_c$=16.7 MPa, which represents only 13.6% of the initial reference dry state strength.

Therefore, for an industrial application such as road aggregate processing, a heat-treatment up to 500 °C is not sufficiently efficient to improve chalk mechanical performance significantly.

Table 4. Mechanical performance of heat-treated Haubourdin chalk samples after 1.5% water re-saturation. Variation in $f_c$ is expressed as a percentage of $f_c$ after heat-treatment (prior to re-saturation).

| **Heat-treatment temperature (°C)** | **$f_c$ before re-saturation (MPa)** | **$f_c$ after re-saturation (MPa)** | **Variation in $f_c$ (%)** |
|---|---|---|---|
| 60 | 14.7 | 10 | 32 |
| 105 | 16.1 | 13 | 19 |
| 200 | 14.7 | 12.6 | 14 |
| 300 | 18.9 | 14.5 | 23 |
| 500 | 21.7 | 16.7 | 23 |

## 3.4. Poro-mechanical investigation

In the following, the poro-mechanical behavior of Haubourdin chalk is investigated during hydrostatic loading, which is closer to the industrial application than uniaxial compression. These experiments also demonstrate both the presence of occluded porosity and the occurrence of pore collapse.

### 3.4.1. Drained and undrained hydrostatic tests

Drained test results are presented in Fig. 12(a) and (b). These highlight the effect of water and of heat-treatment temperature upon the triaxial behavior of chalk. Firstly, in the reference dry state, chalk displays a linear elastic stress–strain relationship up to a so-called pore collapse stress of 20 MPa, corresponding to the stress state when the solid matrix starts to collapse significantly. Above hydrostatic stress $P_c$=20 MPa, strains keep developing with increasing load, so that an irreversible plastic stress–strain behavior is observed, see Fig. 12(a) again.

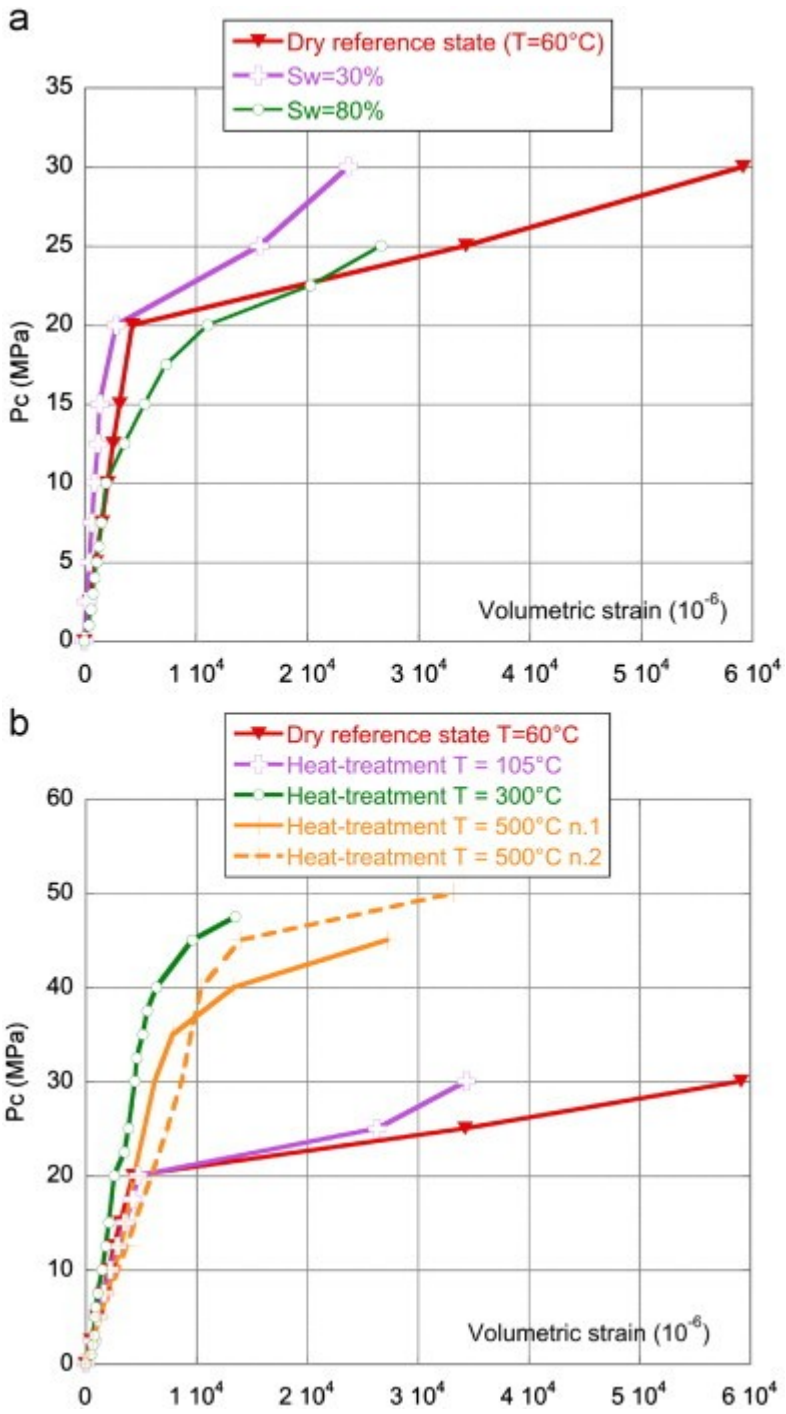


Fig. 12. Drained hydrostatic tests results for (a) dry or partially water-saturated chalk; (b) dry or heat-treated chalk.

For partially water-saturated chalk, Fig. 12(b) shows that pore collapse stress is maintained at a value of 20 MPa at 30% saturation, whereas it is half that value, at 10 MPa, for 80% saturation. In parallel to this, drained bulk modulus $K_b$ is greater at 30% or 80% saturation than in the initial reference dry state, see Table 5. Although each of these results is obtained on a single sample, which means that experimental variability cannot be accurately assessed, they both point to an actual increase in rigidity in presence of partial water saturation. Such effect is not observed in uniaxial compression on Young's modulus $E$: $E$ was assessed as consistently decreasing with increasing water saturation level.

Table 5. Drained bulk modulus $K_b$ was determined in the initial linear elastic phase of our poro-mechanical tests on chalk samples, depending on their state (dry reference state, after heat treatment or partially water saturated). Linear interpolation is performed using the least squares method, and the Pearson coefficient $R^2$ is provided in the third table column.

| **Sample state** | **$K_b$ (MPa)** | **Pearson's coefficient $R^2$** |
|---|---|---|
| Dry reference state (60 °C oven-drying) | 4650–4740 | 0.999 |
| Heat treatment $T$=105 °C | 4140 | 0.998 |
| Heat treatment $T$=300 °C | 6785 | 0.990 |
| Heat treatment $T$=500 °C (sample 1) | 4730 | 0.986 |
| Heat treatment $T$=500 °C (sample 2) | 3650 | 0.993 |
| Partially water-saturated $S_w$=30% | 10,430 | 0.994 |
| Partially water-saturated $S_w$=80% | 5400 | 0.984 |

For heat-treated chalk, no significant change in triaxial stress–strain behavior is observed after 60 and 105 °C heat-treatment. Pore collapse strength is of 20 MPa in both cases. On the opposite, 300 °C and 500 °C heat-treated chalk samples all display a significant increase in pore collapse strength, with a 40 MPa value for $T$=300 °C heat-treatment, and 35–40 MPa for 500 °C heat-treatment. As observed under uniaxial compression, chalk strength is improved by heat-treatment from $T$=300 °C. This is attributed to a strengthening of the solid skeleton of chalk, possibly owing to $CaCO_3$ crystallization from the $Ca^{2+}$ and $CO_3^{2-}$ ions commonly present in chalk interstitial water [10], see Section 4 and Fig. 16. Drained bulk modulus $K_b$ does not evolve monotonously with $T$: $K_b$ is greater than in the initial reference dry state after 300 °C heat-treatment (with a value of 6780 MPa), whereas it ranges between 3650 and 4730 MPa after 500 °C heat-treatment, which corresponds to the range of $K_b$ in the initial reference dry state (4650–4740 MPa). In conclusion, it is estimated that $K_b$ remains on the same order of magnitude even after a heat-treatment up to 500 °C, similar to Young's modulus and Poisson's ratio, which were assessed in uniaxial compression (and which are directly related to $K_b$ by $E/(3(1-2\nu))$). Finally, it is believed that a very limited recrystallisation of calcium carbonate (from the ions present in chalk interstitial water) is bound to have limited effect on the overall chalk rigidity, as measured by $K_b$. Yet, small recrystallisation may help strengthen a few solid skeleton bridges, and delay its collapse under confinement, so that chalk strength alone is improved.

### 3.4.2. Undrained hydrostatic tests

For the two samples tested, one after 60 °C oven-drying and the other after 500 °C heat-treatment, solid matrix bulk modulus $K_s$ is assessed at 40 GPa±2. As recalled by Alam et al. [5], the average solid matrix bulk modulus of pure calcite is of 75 GPa, which is almost twice that assessed in our experiments. This means that Haubourdin chalk, when compared to pure calcite, presents a non-negligible amount of occluded pores, which are not accessible to interstitial fluid. From its $K_s$ value, the Biot coefficient of Haubourdin chalk is derived at a value of 0.88. As a matter of comparison, Kerguelen Plateau chalk has similar porosity and $CaCO_3$ content as Haubourdin chalk [5], and its Biot coefficient is very similar, with values of 0.92–0.93, although it was assessed by an ultrasonic non-destructive method. Such Biot coefficient value, close to 1, testifies of low solid skeleton consolidation.

### 3.4.3. Permeability and porosity under confinement

Finally, a coupled experiment has been conducted on a reference dry Haubourdin chalk sample, providing simultaneously gas permeability and pore volume variation. At given hydrostatic stress $P_C$, both gas permeability and relative pore volume (i.e. porosity) are assessed by different means, yet these show direct evidence of pore collapse for Pc≥20MPa, see Fig. 13. Until this test, we interpret the yield stress limit of the linear elastic behavior under hydrostatic loading as a pore collapse stress. This original experiment shows directly the pore collapse phenomenon and amplitude, by measuring porosity and gas transport change during a hydrostatic stress cycle (i.e. monotonous increase and then decrease), see Fig. 13 again.

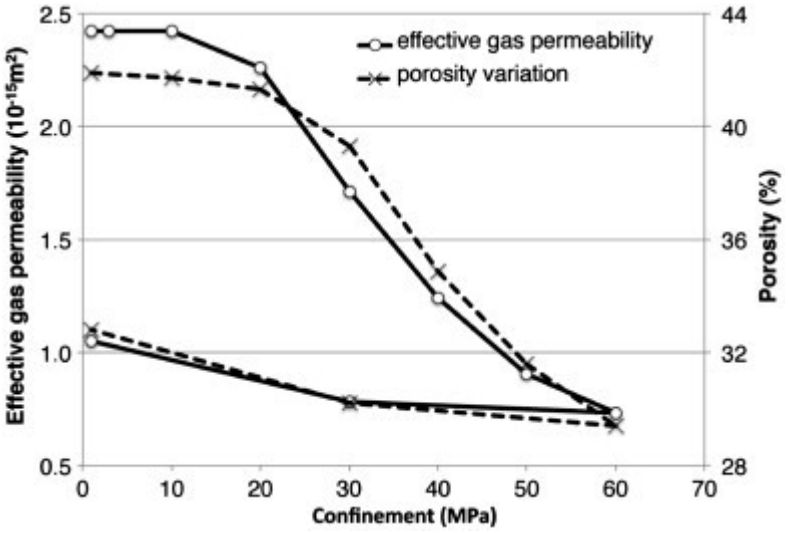


Fig. 13. Gas permeability and pore volume change under increasing confinement for a 60 °C oven-dried Haubourdin chalk sample.

First, it can be observed that porosity and gas permeability $K$ follow similar evolutions with increasing and then decreasing confinement. In particular, a significant decrease in gas permeability (and porosity) is observed from 20 MPa confinement: this is the so-called pore collapse stress. After the loading/unloading cycle, gas permeability and porosity do not recover their initial values: porosity is lower by 21.7%, and $K$ is lower by 56.6%. These are the signs of an irreversible pore collapse.

# 4. Discussion

## 4.1. Comparison with various chalk deposits

### 4.1.1. Microstructure properties

To compare microstructure properties further, basic characteristics of various chalk deposits are provided in Table 6: they originate both from the same sedimentary basin as Haubourdin chalk, i.e. the north European Anglo-Paris Basin [45], which extends to Belgium, Ireland, the North Sea and part of Denmark and Poland [3]), or from a different sedimentary basin (located in the Indian Ocean) [5]. While chalks from the Anglo-Paris basin are buried at no more than 600 m, Kerguelen Plateau chalk is located at 478–555 m below the sea floor. Therefore, unless otherwise stated, the analysis will be primarily focused on Anglo-Paris basin chalks.

Table 6. Comparison of basic microstructure characteristics of various chalk deposits, from the literature [5], [6] and this study (where densities are given by the ethanol saturation method, mineralogical composition by Bernard calcimetry). Ap. stands for apatite, Feld. for feldspar, tit.ox. for titanium oxide and Sm. for smectite.

| **Chalk deposit name, origin, age and reference** | **Apparent dry density ($g/cm^3$)** | **Solid dry density ($g/cm^3$)** | **Specific surface area ($m^2/g$)** | **Porosity $\phi$ (%)** | **Average particle diameter (µm)** | **Gas permeability (mD)** | **$CaCO_3$ content (%)** |
|---|---|---|---|---|---|---|---|
| Beauval, Picardie, France, *Late Santonian*, 85.8 Ma [6] | 1.58 | 2.91 | 6.9 | 45.7 | 0.3 | 26.0 | 56.0 (+Ap.) |
| Hardivillers, Picardie, France, *Late Santonian*, 85.8 Ma [6] | 1.48–1.57 | 2.814–2.8 | 3.1–3.2 | 44.1–47.8 | 0.7 | 10.0–12.3 | 76.5–77.4 (+Ap.) |
| Obourg, Hainaut, Belgium *Campanian*, 83.5 Ma [6] | 1.66 | 2.72 | 3.4 | 39.1 | 0.7 | 1.9 | 94.3 (+Ap.Feld. tit. ox.) |
| St Marguerite s/Mer Normandie, France, *Late Santonian*, 85.8 Ma [6] | 1.47 | 2.73 | 2.1 | 46 | 1.1 | 6.9 | 95.3 (+Feld.) |
| Précy-sur-Oise, Picardie, France, *Campanian*, 83.5 Ma [6] | 1.53 | 2.69 | 1.5 | 43.0 | 1.5 | 7.1 | 100 |
| Haubourdin, France, *Seno-Turonian*, 90 Ma (this study) | 1.57±0.03 | 2.77±0.03 | 1.867–2.137 | 42.0±0.8 | N/A | 2 | 98 ±1 (+Sm.) |
| Kerguelen Plateau, Indian Ocean, *Early Paleocene to Late Campanian*, 62.5–78 Ma [5] | 2.0–2.02 | 2.72 | 3.1–4.7 | 41–42 | N/A | N/A | 91–94.3 |

First, it is observed that chalk deposits close to Haubourdin have hugely varying $CaCO_3$ content, ranging from 56% (Beauval, Picardie, France) to 100% (Précy-sur-Oise, Picardie, France). Except for the latter, French Picardie chalks contain significant amounts of apatite, which is a calcium phosphate, so that these chalks are labelled phosphatic chalks [18], [45]. Such chalks were formed in narrow, 1 km long erosional basins (called *cuvettes*), so that all chalks in the area do not contain significant phosphate amounts [6], as is the case for Précy-sur-Oise and Haubourdin chalks. Owing to its relatively low $CaCO_3$ content, Beauval chalk may rather be labelled as a soft limestone. As for secondary minerals, Normandy St Marguerite S/Mer chalk contains feldspar, and Belgian Obourg chalk contains a mix of apatite, feldspar and titanium oxide. Kerguelen Plateau chalk contains barium sulfate, smectite and varying proportions of natural zeolite. These minerals are bound to affect chalk characteristics. In particular, the greater the $CaCO_3$ content, the greater the average particle diameter: it is of 0.3µm at 56% $CaCO_3$ content, and up to 1.5µm for 100% pure chalk, see [6] and Table 6. This means that heterogeneities induce smaller solid particles.

Also, greater specific surface areas are linked to lower $CaCO_3$ content, all the more so when clay is present, e.g. smectite in Haubourdin chalk. Indeed, high specific surface area has been shown to be linked to clayey or silica content [46], and data on Picardie chalks show that it is also the case with apatite content. This explains that Haubourdin chalk's specific surface area (1.867–2.137 $m^2/g$) is significantly greater than 100% pure $CaCO_3$ Précy-sur-Oise chalk (with a value of 1.5 $m^2/g$). Moreover, Haubourdin and Précy-sur-Oise chalks have very close porosities (43.0 and 42±0.8%). Their gas permeability values are on the same order, although that of Précy-sur-Oise is greater. This is attributed to a difference in measurement techniques: our permeability test is performed under a low confinement pressure (of 4 MPa), which is bound to induce micro-crack closure, i.e. a limited pore volume decrease.

Mortensen et al. [47] have shown that gas permeability $K$ should depend on both porosity and specific surface area: the greater the porosity and the lower the specific surface area $SSA$, the greater the $K$. While porosity provides rough estimate of gas pathway volume, specific surface area is a

measure of gas pathway tortuosity. Such trend is also observed here. In particular, St Marguerite s/Mer and Précy-sur-Oise chalks have very similar permeabilities, with respective values of 6.9 and 7.1 mD, yet St Marguerite s/Mer chalk ($\phi$=46% and *SSA*=2.1 $m^2/g$) has greater porosity than Précy-sur-Oise chalk ($\phi$=43% and *SSA*=1.5 $m^2/g$). The decrease in porosity is counterbalanced by the decrease in gas pathway tortuosity, i.e. in *SSA*. Nevertheless, gas permeability is also greatly influenced by the sample stress state. For instance, gas permeability value of Haubourdin chalk (at 2 mD) is similar to that of Obourg chalk (at 1.9 mD), although Obourg chalk has lower porosity and greater specific surface area ($\phi$=39.1% and *SSA*=3.4 $m^2/g$ vs. $\phi$=42% and *SSA*=1.8-2.1 $m^2/g$): according to Mortensen et al. [47], Obourg chalk should have lower permeability than Haubourdin chalk. As mentioned above, this is explained by the fact that our measurements are conducted under hydrostatic stress (at 4 MPa): such stress state is bound to induce closure of the bigger pores and/or micro-cracks (initially present or created by oven-drying), i.e. closure of the bigger gas pathways.

Finally, it is observed that Haubourdin chalk has very similar microstructure as Kerguelen Plateau chalk, although the latter is located at depths ranging from 478.4 to 554.8 m below sea floor [5]. They have similar porosities (42% for the former and 41–42% for the latter), similar solid dry density (2.77 $g/cm^3$ vs. 2.72 $g/cm^3$), and their specific surface areas are on the same order of magnitude (of 1.8–2.1 $m^2/g$ for Haubourdin chalk and 3.1–4.7 $m^2/g$ for Kerguelen Plateau chalk), see Table 6. Their main recorded difference is that Haubourdin chalk is purer, with 98% $CaCO_3$ (91–94.3% for Kerguelen Plateau). This shows that despite having encountered lower burial and overburden pressures, Haubourdin chalk has a similar microstructure to a more deeply buried, less pure, chalk. This is all the more so remarkable as their compressive strengths are similar (14.7 MPa±1.5 for Haubourdin and 19 MPa±1 for Kerguelen Plateau), see Table 7. It is concluded that, of all chalks found in the literature, Kerguelen Plateau chalk (located in the Indian Ocean, at 478.4–554.8 m below sea floor) has the closest properties to Haubourdin.

Table 7. Mechanical performance of various chalk deposits, from the literature and this study, in the dry state and under uniaxial compressive loading.

| **Chalk deposit name, origin and reference** | **Epoch** | **Average peak stress $f_c$ (MPa)** | **Young's modulus *E* (MPa)** | **Porosity $\phi$ (%)** | **$CaCO_3$ content (%)** |
|---|---|---|---|---|---|
| Upper Yorkshire, Selwicks Bay, England [42] | Upper Cretaceous | 25.6 | 10,900 | 17.7–38.3 | 96–98 |
| Middle Norfolk, Burnham Market, England [42] | Upper Cretaceous | 13.0 | 8000 | 33.2–40.2 | 96–98 |
| Lewes, Bois-de-Cise, France [38] | Upper Cretaceous | 4 | 420 | 41 | - |
| Haubourdin, North, France (this study) | Upper Cretaceous (90 My) | 14.7±1.5 | 10,000 | 42.0±0.8 | 98±1 |
| Kerguelen Plateau, Indian Ocean (this study) | Early Paleocene to Late Campanian (90 My) | 19±1 | N/A | 41–42.0 | 91–94.3 |

### 4.1.2. Mechanical performance

Whereas Kerguelen Plateau chalk is tested through consolidation experiments, several initially dry French and English chalks have been tested in uniaxial compression [38], [42], see Table 7. Both Yorkshire and Norfolk English chalks are almost pure, with a $CaCO_3$ content greater than 96%, which is similar to that of Haubourdin chalk. Despite this, Upper Yorkshire chalk has a significantly greater $f_c$ than Haubourdin chalk and a similar *E*, with average values at 25.6 MPa and 10.9 GPa, respectively (compared with 14.7 MPa and 10.0 GPa for Haubourdin chalk). The greater $f_c$ of

Upper Yorkshire chalk is directly related to its smaller porosity (with an average value ϕaverage=24.4). Despite this, as for Haubourdin chalk, such mechanical performance corresponds to a moderate strength chalk, according to the classification proposed by Franklin et al. [48].

On the opposite, despite porosity values similar to those of Haubourdin chalk (these range from 33.2% to 40.2%, with an average value of 35.1%), Middle Norfolk chalk has a slightly lower compressive strength $f_c$ than Haubourdin: it is 13 MPa on average, ranging between 7.4 and 25.1 MPa. Such huge variations in compressive strength are attributed to a hugely varying porosity ϕ=33.2–40.2. When comparing Middle Norfolk and Haubourdin chalks, it cannot be concluded that lower porosity corresponds to greater strength. Rather, it is concluded that porosity is not the only parameter affecting chalk mechanical strength. It is also related to the extent of compaction, cementation or recrystallisation of its solid grains, all related to diagenesis. As noted by Bell et al. [42], Middle Norfolk chalk has undergone limited diagenetic processes, in particular low calcite precipitation and cementation. This is obviously also the case for weak French Lewes chalk, which has only 4 MPa strength and 420 MPa Young's modulus, despite comparable porosity to Haubourdin chalk, see Table 7.

## 4.2. Partially water-saturated chalk: physical phenomena at the origin of the water weakening effect

One first explanation of the water-weakening effect of chalk generally assumes the existence of water films between calcite grains in the initial “dry” state [10]: Lord et al. [44] have shown that adsorbed water is present in chalk up to 300 °C, even in very small amounts; so-called structural water is released at temperatures above 300 °C only. At room temperature, when ambient air relative humidity is increased, these structural water films transform into menisci. These increase in size and curvature radii from very low water saturation levels, so that associated capillary forces decrease, which leads to mechanical weakening of chalk [1], [49].

The validity of this explanation is described by a simple model. Its main assumption consists in isolating two calcite grains, and considers that there is no cementation between them. As shown in Section 3.4, Biot coefficient $b$ measures a rigidity ratio between the bulk of the material ($K_b$) and the solid skeleton ($K_s$). At a value of 1, it means that there is no contact cementation between individual grains (i.e. it is a granular material). At a value of 0.88 (as is the case for Haubourdin chalk), it is still assumed that grain cementation is present, yet not between a majority of grains in the chalk, so that the following calculation focuses more on non-cemented grains, than on the cemented part of the chalk.

In the following, the two considered calcite grains are represented as two spheres of identical radius $R$, in contact due to a capillary water meniscus of thickness $2h \ll R$, of width $2a \gg 2r$ and of curvature radius $r$. In such instance, Andreotti et al. [50] show that the cohesive force between the grains has the following expression (on the first order):(6)$F_{cap} \approx 2\pi\gamma R\cos\theta$where γ is the surface tension between water and air, and θ is the contact angle (it is zero for a perfectly wetting fluid such as water), see Fig. 14. In this expression, the surface tension at the perimeter between the water meniscus and the spheres is neglected. Per unit area, this force is simply converted to a stress $\sigma_{cap}=F_{cap}/(\pi a2)$. In a first instance, Risnes et al. [51] propose a simplified assessment of σcap by assuming that it acts roughly on a square surface with side length $2R$: for water in contact with the two spherical chalk grains: $\sigma_{cap} \approx (\pi/2R)\gamma$. For an average grain size of 1μm and with water/air surface tension $\gamma=73\times10-3$N/m at 20 °C, the corresponding stress level is of 0.2 MPa (the

corresponding tensile force is of $2.3\times10^{-7}$ N): this represents a very low contribution to grain cohesion at low water content. Nevertheless, at extremely low water content, $r$ and $a$ tend towards zero, so that the surface area on which $F_{cap}$ acts also tends towards zero. The assumption of a square surface of side length $2R$ is no longer valid. When it is assumed that the lowest water content possible has a water meniscus, at least seven to ten water molecules must be in parallel, each having a diameter of ca. 0.3 nm [52], [19]: below such values, no water film exists at the grain surface, and adsorption phenomena are predominant. This corresponds to 2h≈3nm (ten water molecules in parallel), i.e. as 2h≈a2/R, one gets a2≈R×3×10−9m2. For grains of diameter 1μm, σcap is then of 153 MPa. This is no longer negligible to explain the increase in strength of chalk at extremely low water content, e.g. after 60 °C oven-drying. The significant decrease of σcap down to 0.2 MPa for greater water content (as calculated by [51], by assuming that a≈R) means that the decrease in capillary force represents up to four orders of magnitudes, which is huge and may suffice to explain water weakening. Nevertheless, it should be noted that this calculation accounts for the variation in $f_c$ with decreasing water content , yet not in Young's modulus $E$.

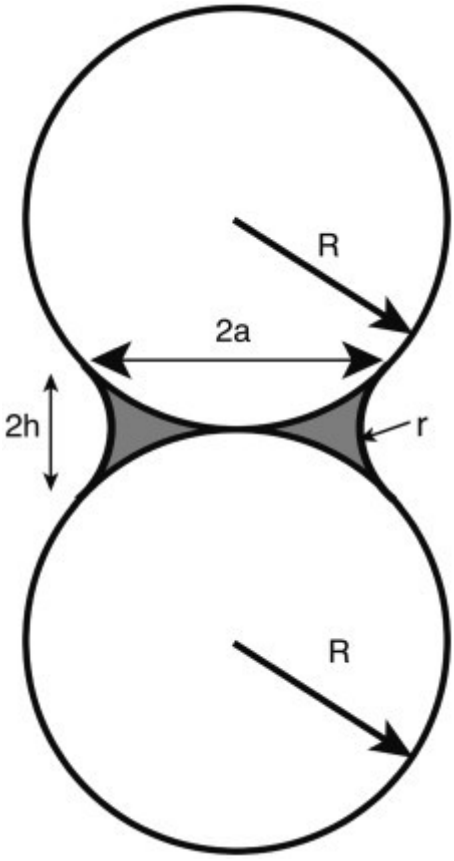


Fig. 14. Sketch of water menisci present between two idealized spherical chalk grains of identical radius $R$.

A second possible explanation for water weakening of chalk would be that water films have a lubricating effect at the interface between calcite grains [53], which eases local straining and collapse; this effect would be enhanced in presence of a greater water amount. Whereas this second interpretation still requires experimental validation, a third argument has been partially validated by Heggheim et al. [10]. Water weakening of chalks is interpreted as being due to dissolution/diffusion phenomena at the chalk grain interface, triggered by local pressure [10], as modelled in [54]. Some degree of $CaCO_3$ dissolution is also assumed between the individual chalk grains by Mata [9]. Yet, owing to the very low solubility of $CaCO_3$ into water (its solubility product is $K_s(CaCO_3)=3.8\times10^{-9}$

at 20 °C, to compare to that of $NaCl_s$, which is $K_s(NaCl)=38.98$), this effect is bound to be very limited, see Risnes et al. [40].

Furthermore, water-weakening of chalk should be considered rather as liquid-weakening of chalk, as it depends strongly on the liquid fluid nature [55], [8], [1]: the mechanical strength of dry chalk is greater than that of chalk saturated with oil, which is itself greater than that of chalk saturated with methanol, the lowest strength being obtained with water. To explain this, Risnes et al. [40] have related water activity to chalk strength: chalk strength decreases when water activity increases. Water activity represents the ratio between water vapor pressure and saturating water vapor pressure at the same temperature. Alternately, experiments by Schroeder et al. [8] have suggested that the polarizing ability of the liquid used to saturate chalk pores has an effect on its weakening amplitude: this would be an effect of electrostatic forces, acting at the level of grains and their interfaces.

## 4.3. Physical phenomena at the origin of the heat-hardening effect

The removal of structural water within chalk has been accounted for in the case of heatings up to 300 °C [44], [10]. This could be attributed to structural water being actually removed from the clayey minerals present in chalk. The main clayey component of Haubourdin chalk is smectite (by 95%), see Section 3.1.1. By using literature analysis and TGA experiments, Brown et al. [56] show that smectites lose interlayer water between 110 °C and 450 °C: the main decomposition peak is at ca. 230 °C for a typical montmorillonite (from Yavapai, Arizona, USA). Therefore, up to 300 °C heating, the removal of structural water could originate from the clay mineral present in Haubourdin chalk. This statement is no longer valid for other types of clay, e.g. kaolinite or illite, see [57].

This loss of structural water is an explanation for the increase in compressive strength of Haubourdin chalk with increasing heat-treatment temperature, mainly above 100 °C. To validate this interpretation, 60 °C oven-dried chalk has been powdered and analyzed by TGA. A single peak in mass loss derivative is observed, which ranges between 760 and 840 °C (with an average value at 795.5 °C) depending on the sample considered, see Fig. 15(a) for an example at 815 °C. It is attributed to calcium carbonate decarbonation [13]. No other peak, at a lower temperature, is observed, which would be attributable to the loss of structural water. Therefore, unless if this occurs in very limited amounts (below 0.01 mg, i.e. below 0.02% of the sample initial mass), as would be the case if corresponding to clay decomposition, this argument must be rejected to explain the increase in strength with increasing heat-treatment.

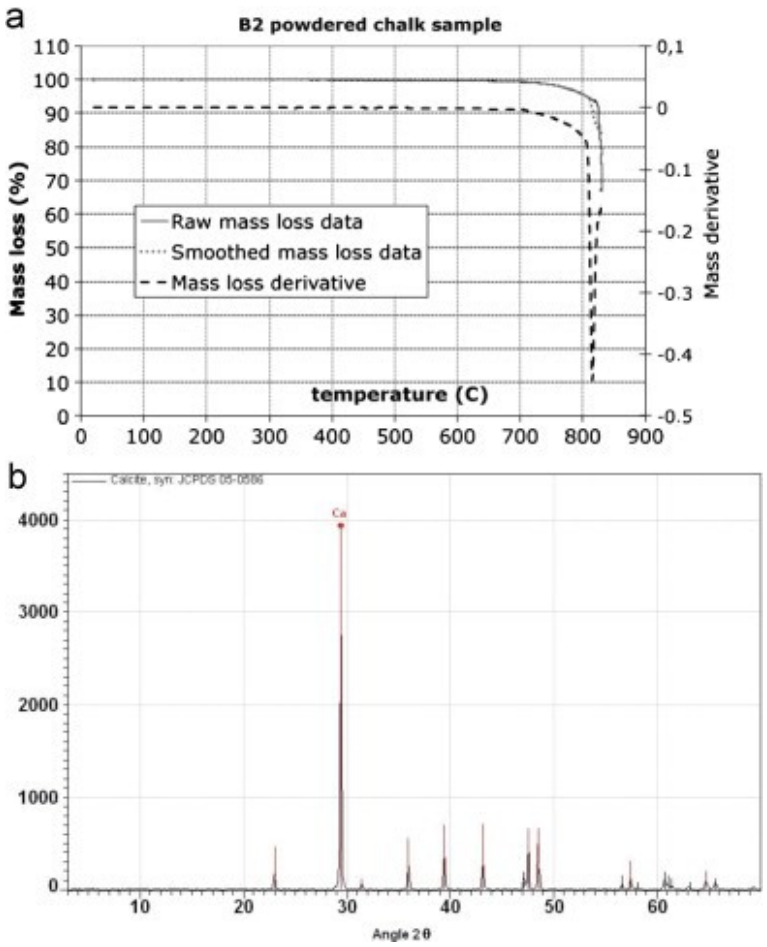


Fig. 15. (a) Example of thermogravimetry analysis (TGA) of powdered Haubourdin chalk preliminary oven-dried at 60 °C. Six different samples have been tested with identical results. (b) Diffractogram obtained by XRD on a thin oriented slice of Haubourdin chalk.

Another possibility is that $CaCO_3$ may be present in Haubourdin chalk in both calcite and aragonite forms. Indeed, mineral pure aragonite (of biogenetic origin) changes crystallographic form (to calcite phase) from 470 °C [58] (as does coral aragonite at 300 °C). As Bell et al. recall [42], when aragonite is converted to calcite, the associated increase of ca. 8% by volume makes a significant supply of cement available, able to bond solid particles together: this will induce solid skeleton strengthening at a greater scale than that of the individual crystals. Although no aragonite is observed in the XRD analysis of Haubourdin chalk, see Fig. 15(b), aragonite presence may be shadowed by that of greater amounts of calcite [58]. Nevertheless, aragonite is reputed being a relatively short-lived mineral, so that, owing to the age of Haubourdin chalk (on the order of 90 Ma), its presence is rather unlikely. Therefore, despite several positive arguments, it is thought that aragonite presence is not the main reason for chalk heat-hardening.

A more plausible chemical origin for the increase in chalk strength with heat-treatment is recrystallisation of calcium carbonate from pore water, due to water evaporation [10]. In order to prove this, de-ionised water was used to saturate a chalk sample for at least 30 days; a few drops of this water was extracted from the sample, deposited on a steel plate (of a few centimeter square area) and placed in an oven at 105 °C until full drying. A solid deposit forms on the steel plate surface, which is observed with the SEM. EDS analysis shows that this deposit is made of calcium carbonate. Therefore, this experiment indicates that whenever a chalk sample is heat-treated, a certain amount of calcium carbonate is deposited by recrystallisation from the pore water on to the

chalk solid skeleton. In further support to this, and despite being clearly located inside a hollow micro-fossil, crystals of calcium carbonate have been observed with the SEM in a capillary pore of a 24 h 500 °C heat-treated chalk sample, see Fig. 16. During the extensive SEM analysis of Haubourdin chalk, prior to heat treatment, no such hexagonal crystals were observed. These are present in very limited amount in heat-treated chalk, and analyzed as calcium carbonate by the EDS. Nevertheless, unlike calcium carbonate deposited on a steel plate (see above), the actual formation of these crystals during heat-treatment or incipient cementation (diagenesis) still requires further investigation.

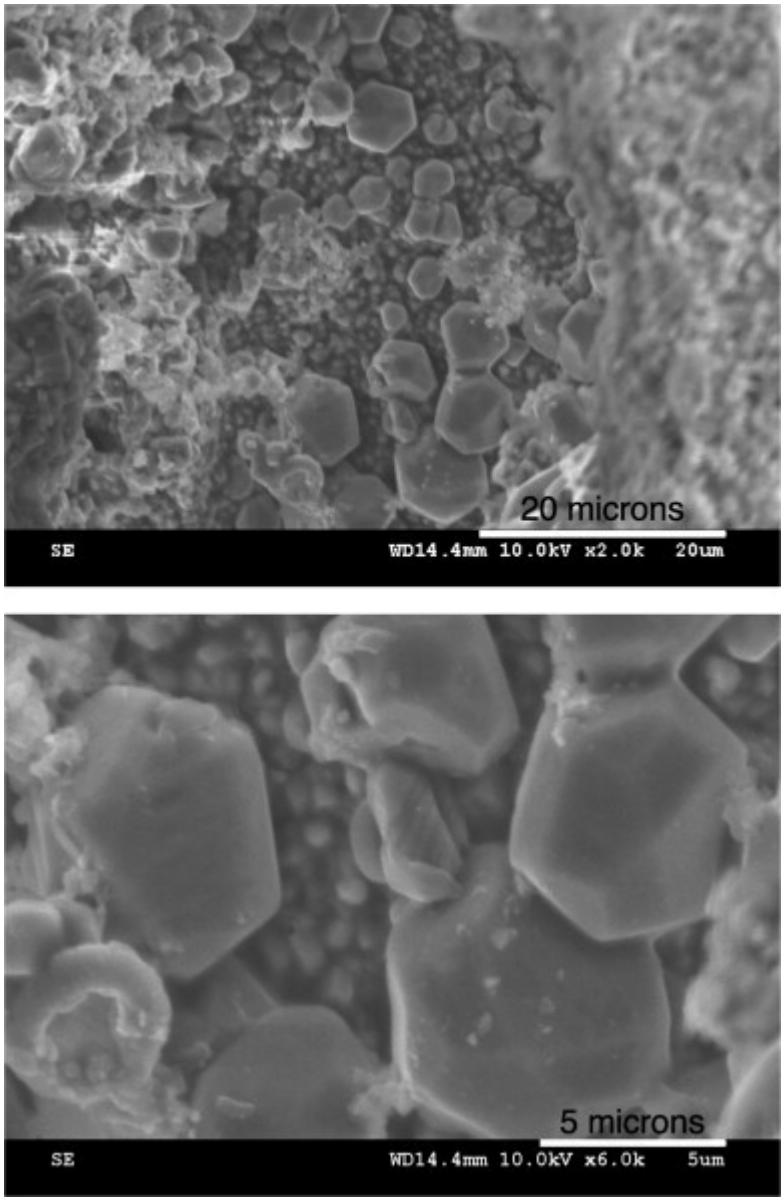


Fig. 16. SEM observations of newly formed $CaCO_3$ crystals (SE detector for the image, BSE detector+EDS analysis for mineralogical composition of crystals) inside a capillary pore of Haubourdin chalk heat-treated up to 500 °C. It clearly corresponds to the inside of a hollow micro-fossil, with incipient cementation, either due to heat-treatment or to diagenesis. No such crystals have been observed on 60 °C oven-dried chalk.

# 5. Conclusion

Haubourdin chalk microstructure and mechanical performance have been assessed in a so-called reference dry state, after 60 °C oven-drying.

With an average porosity $\phi$=42.0±0.8 measured by MIP, and a $CaCO_3$ content of 98%±1, Haubourdin chalk is a highly porous, almost pure chalk. The analysis of 2D SEM images provides a close porosity value of 43.0%±0.9, and a peak pore size of 0.8µm. Haubourdin chalk is classified as a Wackestone, according to Dunham classification [35]. Microstructure assessment also shows that Haubourdin chalk has undergone very limited diagenesis processes (i.e. compaction, recrystallisation or cementation).

In uniaxial compression, Haubourdin chalk has an average strength $f_c$=14.7 MPa±1.5 and Young's modulus $E$=10 GPa, Poisson's ratio $\nu$=0.2, which place it within the category of moderate strength chalks.

Water presence inside its pores induces the so-called water-weakening effect, so that Haubourdin chalk loses up to 45% of its initial reference dry strength at $S_w$=100% saturation (with an average value $f_c$=8.36 MPa, calculated on 10 different samples). For $E$, the decrease at $S_w$=100% is of 15% (with $E$=8452 MPa, result for one single sample). A simple modeling of capillary forces between two calcite spheres, in presence of a water meniscus, shows that capillary pressure variations suffice to explain the water weakening effect, with values up to 153 MPa at the lowest water content (corresponding to a meniscus made of ten water molecules in parallel). Nevertheless, this does not explain the decrease in Young modulus with increasing $S_w$. Several other possible reasons are presented in the manuscript, e.g. the effect of electrostatic forces, acting at the level of grains and their interfaces. Validating these experimentally would require further (and delicate) investigation at a microscopic scale.

After heat-treatment, uniaxial compressive strength $f_c$ increases significantly from 300 °C, so as to reach a value of 21.7 MPa on average after 500 °C heat-treatment: this is a so-called “heat hardening effect”. It represents a huge 47.6% increase in the average strength measured in the reference dry state. Contrarily to $f_c$, the Young modulus and the Poisson ratio are not significantly altered by this phenomenon. From these results alone, heat-treatment can be seen as providing an improvement of chalk mechanical strength, as sought by road building companies. It is mainly attributed to recrystallisation of calcium carbonate from pore water, due to water evaporation during heating. Nevertheless, after a small 1.5% re-saturation, 500 °C heat-treated chalk recovers a strength of 16.7 MPa, which is very similar to that before heat treatment (i.e. in the reference dry state).

Finally, triaxial drained and undrained tests have been conducted on Haubourdin chalk: a yield stress of 20 MPa is identified, which is doubled after a 500 °C heat-treatment, and divided by two for 80% water saturated material. Drained bulk modulus $K_b$ remains on the same order of magnitude after heat treatment, with an average value of 4780 MPa, and it increases in the partial saturated state (when compared to its value in the reference dry state). Solid matrix bulk modulus is identified at 40 GPa, on both 60 °C and 500 °C heat-treated chalk, so that the Biot modulus is derived at a value of 0.88. This is in good agreement with the value of the Biot coefficient for a chalk from a different deposit (Indian Ocean), yet with similar porosity and $CaCO_3$ content. Coupled gas permeability and porosity experiment under hydrostatic stress $P_c$ allow to assess directly the pore collapse amplitude for $P_c$ up to 60 MPa.

# Acknowledgments

The authors wish to thank Eurovia/Groupe Vinci (France) for funding this research, and Prof. Nigel Quayle (Ecole Centrale de Lille, France) for editing our manuscript.

# References

[1] Delage P, Cui YJ, Schroeder C. Subsidence and capillary effects in chalk. In: Balkema, (Ed.), Proceedings of Eurock 96 symposium. Rotterdam, The Netherlands; 1996. ISBN 9054108436.
[2] M. Borre, I.L. Fabricius Chemical and mechanical processes during burial diagenesis of chalk: an interpretation based on specific surface data of deep-sea sediments Sedimentology, 45 (1998), pp. 755-769
[3] Schroeder C. Du coccolithe au réservoir pétrolier, Thèse de Doctorat (PhD thesis, in French), University of Liège, Belgium; 1994.
[4] S. Homand, J.F. Shao Mechanical behaviour of a porous chalk and effect of saturating fluid Mech Cohesive-Frictional Mater, 5 (7) (2000), pp. 583-606
[5] M.M. Alam, M.K. Borre, I.L. Fabricius, K. Hedegaard, B. Røgen, Z. Hossain, *et al.* Biot's coefficient as an indicator of strength and porosity reduction: Calcareous sediments from Kerguelen Plateau J Petrol Sci Eng, 70 (2012), pp. 282-297
[6] M.L. Hjuler, I.L. Fabricius Engineering properties of chalk related to diagenetic variations of upper cretaceous onshore and offshore chalk in the north sea area J Petrol Sci Eng, 68 (2009), pp. 151-170
[7] D.S. Wray, A.S. Gale The palaeoenvironment and stratigraphy of Late Cretaceous Chalks Proc Geol Assoc, 117 (2006), pp. 145-162
[8] Schroeder C. Le pore collapse: aspect particulier de l'interaction fluide squelette dans les craies? In: Proceedings of the international colloquium Craies et Schistes – Bruxelles 20–21 Mars, 1995 [in French].
[9] Mata C. Etude expérimentale et modélisation mécanique des effets du balayage à l'eau dans une craie saturée d Ohuile: application à l'industrie pétrolière. Thèse de Doctorat, PhD thesis, Ecole Nationale des Ponts et Chaussées, France; 2001 [in French].
[10] T. Heggheim, M.V. Madland, R. Risnes, T. Austad A chemical induced enhanced weakening of chalk by seawater J Petrol Sci Eng, 46 (2005), pp. 171-184
[11] D'Hem P. Stabilisation of chalk in north-west France. In: Proceedings of the international chalk symposium. Brighton: Thomas Telford Press, London; 1989. p. 449–56.
[12] Nadah J. Valorisation d'une craie du Nord de la France en assise de chaussée routière. Thèse de Doctorat, PhD thesis, Ecole Centrale de Lille and University of Lille, France; 2009. [in French]
[13] Mounanga P. Etude expérimentale du comportement de pâtes de ciment au très jeune âge: hydratation, retraits, propriétés thermophysiques. Thèse de doctorat de l'Université de Nantes, PhD thesis; 2003 [in French].
[14] Ziegler PA. Geological atlas of Western and Central Europe. Shell International Petroleum Maatschappij B.V., Geological Society of London. Elsevier, Amsterdam; 1990. p. 239.
[15] A.S. Gale, P.A. Jeffery, J.M. Huggett, P. Connolly Eocene inversion history of the Sandown Pericline, Isle of Wight, Southern England J Geol Soc London, 156 (1999), pp. 327-339
[16] SETRA LCPC. Guide technique de réalisation des remblais et des couches de forme. Guides du LCPC, 2ème édition, juillet; 2000.

[17] Centre d'Etudes Techniques de l'Equipement Nord Picardie. Identification géotechnique de la craie d'Haubourdin pour S.A Recynor. CETE Report; 2000 [in French].
[18] I. Jarvis, Sedimentology geochemistry and origin of phosphatic chalks: the Upper Cretaceous deposits of NW Europe Sedimentology, 39 (1992), pp. 55-97
[19] F.N.G. Brue, C.A. Davy, F. Skoczylas, N. Burlion, X. Bourbon Effect of temperature on the water retention properties of two high performance concretes Cem Concr Res, 42 (2012), pp. 384-396
[20] M. Price, R.G. Low, C. Mc Cann Mechanisms of water storage and flow in the unsaturated zone of the chalk aquifer J Hydrol, 233 (2000), pp. 54-71
[21] L. Holzer, F. Indutnyi, Ph. Gasser, B. Munch, M. Wegmann Three-dimensional analysis of porous batio$_3$ ceramics using FIB nanotomography J Microsc, 216 (2004), pp. 84-95
[22] J.N. Kapur, P.K. Sahoo, A.C.K. Wong A new method for gray-level picture thresholding using the entropy of the histogram Graph Models Image Process, 29 (3) (1985), pp. 273-285
[23] T.W. Ridler, S. Calvard Picture thresholding using an iterative selection method
IEEE Trans Syst Man Cybern, 8 (1978), pp. 630-632
[24] W. Tsai Moment-preserving thresholding: a new approach Comput Vis Graph Image Process, 29 (1985), pp. 377-393
[25] N. Otsu A threshold selection method from gray-level histograms IEEE Trans Syst Man Cybern, 9 (1979), pp. 62-66
[26] L.K. Huang, M.-J.J. Wang Image thresholding by minimizing the measure of fuzziness Pattern Recognition, 28 (1) (1995), pp. 41-51
[27] C. Igathinathane, L.O. Pordesimo, E.P. Columbus, W.D. Batchelor, S.R. Methuku Shape identification and particle size distribution from basic shape parameters using Image J Powder Technol, 63 (2008), pp. 168-182
[28] X.T. Chen, C.A. Davy, F. Skoczylas, J.F. Shao Effect of heat-treatment and hydrostatic loading upon the poro-elastic properties of a mortar Cem Concr Res, 39 (2009), pp. 195-205
[29] O. Coussy Poromechanics J. Wiley & Sons, New York (2004)
[30] A. Nur, J.D. Byerlee An exact effective stress law for elastic deformation of rock with fluids
J Geophys Res, 76 (26) (1971), pp. 6414-6419
[31] Y. Benachour, C.A. Davy, F. Skoczylas, H. Houari Effect of high calcite filler addition upon microstructural, mechanical, shrinkage and transport properties of a mortar Cem Concr Res, 38 (2008), pp. 727-736
[32] X.T. Chen, Th. Rougelot, C.A. Davy, W. Chen, F. Agostini, F. Skoczylas, *et al.* Experimental evidence of a moisture clog effect in cement-based materials under temperature Cem Concr Res, 39 (12) (2009), pp. 1139-1148
[33] Chen XT, Caratini G, Davy CA, Troadec D, Skoczylas F, Dormieux L. Coupled transport and poro-mechanical properties of a heat-treated mortar under confinement, Cem Concr Res, under revision
[34] Mortimore RN. Chalk or chalk? In: Proceedings of the international chalk symposium, Brighton. London : Thomas Telford Press; 1989. p. 15–45.
[35] Dunham RJ. Classification of carbonate rocks according to depositional texture. In: Ham (Ed.), Classification of carbonate rocks. Memoir 1, AAPG; 1962. p. 108–121.
[36] A.J. Mallon, R.E. Swarbrick Diagenetic characteristics of low permeability, non-reservoir chalks from the central north sea Mar Petrol Geol, 25 (2008), pp. 1097-1108
[37] S. Diamond Mercury porosimetry: an inappropriate method for the measurement of pore size distributions in cement-based materials Cem Concr Res, 30 (2000), pp. 1517-1525

[38] A. Duperret, S. Taibi, R.N. Mortimore, M. Daigneault Effect of groundwater and sea weathering cycles on the strength of chalk rock from unstable coastal cliffs of NW France
Eng Geol, 78 (2005), pp. 321-343
[39] R.I. Korsnes, E. Wersland, T. Austad, M.V. Madland Anisotropy in chalk studied by rock mechanics J Petrol Sci Eng, 62 (2008), pp. 28-35
[40] R. Risnes, M.V. Madland, M. Hole, N.K. Kwabiah Water weakening of chalk – mechanical effects of water-glycol mixtures J Petrol Sci Eng, 48 (2005), pp. 21-36
[41] R.I. Korsnes, M.V. Madland, T. Austad, S. Haver, G. Røsland The effects of temperature on the water weakening of chalk by seawater J Petrol Sci Eng, 60 (2008), pp. 183-193
[42] F.G. Bell, M.G. Culshaw, J.C. Cripps A review of selected engineering geological characteristics of English Chalk Eng Geol, 54 (1999), pp. 237-269
[43] Madland MV. Capillary effects in high porosity chalk. Thesis for the siv. ing. degree, Stavanger University College, Norway; 1999.
[44] Lord CJ, Rhett DW, Johlman CL. Is capillary suction a viable cohesive mechanism in chalk? In: Eurorock'98, Trondheim, Norway; 1998.
[45] I. Jarvis The Santonian–Campanian phosphatic chalks of England and France Proc Geol Assoc, 117 (2006), pp. 219-237
[46] B. Røgen, I.L. Fabricius Influence of clay and silica on permeability and capillary entry pressure of chalk reservoirs in the North Sea Pet Geosci, 8 (2002), pp. 287-293
[47] J. Mortensen, F. Engstrøm, I. Lind The relation among porosity, permeability and specific surface of chalk from the Gorm Field, Danish North Sea SPE Reservoir Eval Eng, 1 (1998), pp. 245-251
[48] J.A. Franklin, E. Broch The point load strength test Int J Rock Mech Min Sci, 9 (1972), pp. 669-697
[49] Schroeder C, Shao JF. Plastic deformation and capillary effects in chalks. In: Proceedings of the 5th North Sea Chalk Symposium, Reims, France; 1996.
[50] Andreotti B, Forterre Y, Pouliquen O. Les milieux granulaires – entre fluide et solide. EDP Sciences, France; 2011. ISBN: 978-2-7598-0097-1.
[51] R. Risnes, H. Haghighi, R.I. Korsnes, O. Natvik Chalk fluid interactions with glycol and brines Tectonophysics, 370 (2003), pp. 213-226
[52] O. Kadlec, M.M. Dubinin Comments on the limit of applicability of the mechanism of capillary condensation J Colloid Interface Sci, 31 (4) (1969), pp. 479-489
[53] K.L. Johnson Contact mechanics Cambridge University Press, UK (1987)
[54] D. Lydzba, S. Pietruszczak, J.F. Shao Intergranular pressure solution in chalk: a multi scale approach Comput Geotech, 34 (2007), pp. 291-305
[55] R. Risnes Deformation and yield in high porosity outcrop chalk Phys Chem Earth, 26 (2001), pp. 53-57
[56] I.W.M. Brown, K.J.D. MacKenzie, R.H. Meinhold The thermal reactions of montmorillonite studied by high-resolution solid-state $^{29}$Si and $^{27}$Ai NMR J Mater Sci, 22 (1987), pp. 3265-3275
[57] R. Fernandez, F. Martirena, K.L. Scrivener The origin of the pozzolanic activity of calcined clay minerals: a comparison between kaolinite, illite and montmorillonite Cem Concr Res, 41 (2011), pp. 113-122
[58] J.L. Irigaray, H. Oudadesse, H. El Fadl, T. Sauvage, G. Thomas, A.M. Vernay Effet de la température sur la structure cristalline d'un biocorail J Therm Anal, 39 (1993), pp. 3-14